J Physiol 594.15 (2016) pp 4225–4251

The Journal of Physiology

Single cell transcriptome analysis of mouse carotid body glomus cells

Ting Zhou[1,*], Ming-Shan Chien[1,*], Safa Kaleem[1] and Hiroaki Matsunami[1,2]

[1] *Department of Molecular Genetics and Microbiology, Duke University Medical Centre, Durham, NC, USA*
[2] *Department of Neurobiology and Duke Institute for Brain Sciences, Duke University, Durham, NC, USA*

Key points

- Carotid body (CB) glomus cells mediate acute oxygen sensing and the initiation of the hypoxic ventilatory response, yet the gene expression profile of these cells is not available.
- We demonstrate that the single cell RNA-Seq method is a powerful tool for identifying highly expressed genes in CB glomus cells.
- Our single cell RNA-Seq results characterized novel CB glomus cell genes, including members of the G protein-coupled receptor signalling pathway, ion channels and atypical mitochondrial electron transport chain subunits.
- A heterologous cell-based screening identified acetate (which is known to affect CB glomus cell activity) as an agonist for the most highly abundant G protein-coupled receptor (Olfr78) in CB glomus cells.
- These data established the first transcriptome profile of CB glomus cells, highlighting genes with potential implications in CB chemosensory function.

Abstract The carotid body (CB) is a major arterial chemoreceptor containing glomus cells whose activities are regulated by changes in arterial blood content, including oxygen. Despite significant advancements in the characterization of their physiological properties, our understanding of the underlying molecular machinery and signalling pathway in CB glomus cells is still limited. To overcome this, we employed the single cell RNA-Seq method by performing next-generation sequencing on single glomus cell-derived cDNAs to eliminate contamination of genes derived from other cell types present in the CB. Using this method, we identified a set of genes abundantly expressed in glomus cells, which contained novel glomus cell-specific genes. Transcriptome and subsequent *in situ* hybridization and immunohistochemistry analyses identified abundant G protein-coupled receptor signalling pathway components and various types of ion channels, as well as members of the hypoxia-inducible factors pathway. A short-chain fatty acid olfactory receptor Olfr78, recently implicated in CB function, was the most abundant G protein-coupled receptor. Two atypical mitochondrial electron transport chain subunits (Ndufa4l2 and Cox4i2) were among the most specifically expressed genes in CB glomus cells, highlighting their potential roles in mitochondria-mediated oxygen sensing. The wealth of information provided by the present study offers a valuable foundation for identifying molecules functioning in the CB.

(Resubmitted 6 December 2015; accepted after revision 24 February 2016; first published online 4 March 2016)
Corresponding author H. Matsunami: 264 CARL Building, Box 3054, Duke University Medical Centre, Durham, N.C. 27710, USA. Email: hiroaki.matsunami@duke.edu

*These authors contributed equally to this work.

DOI: 10.1113/JP271936

Abbreviations AMPK, AMP-activated protein kinase; CB, carotid body; DIG, digoxigenin; ETC, electron transport chain; GPCR, G protein-coupled receptor; HIF, hypoxia-inducible factor; OSN, olfactory sensory neuron; PACAP, pituitary adenylate cyclase-activating polypeptide; PBS, phosphate-buffered saline; PFA, paraformaldehyde; PKA, protein kinase A; PKC, protein kinase C; ROS, reactive oxygen species; RPM, the number of reads mapped to each gene per million of total mapped reads; SCFA, short chain fatty acid; VSN, vomeronasal sensory neuron.

Introduction

Oxygen is essential to the survival of animals, and deviation from its normal homeostasis state may lead to undesirable consequences or even death. At the cellular or tissue level, a reduction in the oxygen level can be sensed via stabilization of hypoxia-inducible factors (HIFs), which initiate transcriptions of various hypoxia responsive genes to facilitate survival under a hypoxic state (Semenza, 2012). At the systemic level, even a moderate drop in oxygen tension, at a level that could go undetected by most cells, immediately activates the carotid body (CB) located at the carotid artery bifurcations (Lopez-Barneo *et al.* 2009; Prabhakar, 2013). The CB reacts to drops in arterial oxygen tension by instructing the brain stem respiratory centre to engage in reflex hyperventilation. Such sensitive and immediate responses are crucial for the prevention of more widespread hypoxemia. Enhanced CB activity has also been implicated in sympathetic activation leading to heart rate variability and hypertension among patients with obstructive sleep apnoea and chronic heart failure (Schultz & Li, 2007; Dempsey *et al.* 2012).

Despite great physiological significance, the identity of oxygen sensors functioning in the CB is still controversial, although multiple players have recently been shown to be critical in this process (Peng *et al.* 2010; Chang *et al.* 2015; Fernandez-Aguera *et al.* 2015; Yuan *et al.* 2015). A long-held theory suggests that the CB glomus cells, also known as Type I cells, sense hypoxia through hampered mitochondria metabolism (Mills & Jobsis, 1970, 1972; Duchen & Biscoe, 1992*a*,*b*; Streller *et al.* 2002; Buckler & Turner, 2013), although how their mitochondria are specifically influenced by moderate hypoxia is not understood (Chandel & Schumacker, 2000; Kemp & Telezhkin, 2014). To complicate things further, we do not fully understand how the hypoxia signal is transduced to downstream ion channels important for cellular depolarization. In addition to oxygen, CB glomus cell activity is affected by CO_2, pH, glucose, insulin and acetate (Sato, 1994; Pardal & Lopez-Barneo, 2002; Ribeiro *et al.* 2013; Prabhakhar & Joyner, 2014), although the molecules mediating these effects are not well characterized.

To better understand CB transduction pathways, a comprehensive list of genes expressed in CB glomus cells would serve as a useful resource. However, it has proved challenging to conduct molecular biology experiments, at least partly as a result of the extremely small size of the CB (several hundred micrometers in diameter in rodents). Currently available CB transcriptome information is obtained from whole CB tissues (Ganfornina *et al.* 2005; Balbir *et al.* 2007; Fagerlund *et al.* 2010; Mkrtchian *et al.* 2012; Chang *et al.* 2015), which may contain other cell types, including sustentacular cells, endothelial cells, connective tissue cells, fat cells and circulating immune cells.

In the present study, we employed a more targeted approach to focus on glomus cells using the single cell RNA-Seq method. Using this approach, we not only confirmed the presence of many of the known CB genes, but also uncovered a large set of genes abundantly expressed in CB glomus cells. Our data suggest that CB glomus cells have a unique transcriptome profile, prominently expressing G protein-coupled receptor (GPCR) signalling pathway components, ion channels and HIF target genes. An olfactory receptor, Olfr78, was the most abundant GPCR in CB glomus cells and responded to acetate in heterologous cells, supporting recent findings suggesting that Olfr78 is enriched in CB and plays an important role in CB function (Chang *et al.* 2015). The present study also uncovered two atypical mitochondrial electron transport chain (ETC) subunits (Ndufa4l2 and Cox4i2) that were highly enriched in CB glomus cells compared to multiple mouse tissues, highlighting their potential roles in mitochondria-mediated oxygen sensing.

Methods

Ethical approval and tissue collection

All experiments involving animals were carried out in accordance with the Institutional Animal Care & Use Committee of Duke University Medical Centre, Durham, NC, USA. Adult C57BL6/J, SPRET/EiJ, CASTS/EiJ and Olfr78^{tm1Mom}/MomJ mice were obtained from the Jackson Laboratory (Bar Harbor, ME, USA). For each CB glomus cell isolation experiment, four mouse pups (postnatal day 4 or 5) from the same litter were used. Seven out of eight CB glomus cells sequenced derived from the C57Bl6/J strain, and the other one derived from a C57Bl6/J × SPRET/EiJ cross. The pups were anaesthetized by hypothermia on ice for 10 min followed by immediate decapitation and tissue collection. For the single cell isolation of olfactory sensory neurons (OSNs) and vomeronasal sensory neurons (OSNs), 3-week-old mice were used. Adult mice were euthanized using CO_2 according to the

approved animal protocol. To collect CB for histology experiments, the carotid artery bifurcations from mice 3 weeks or older (male and female) were snap frozen in Tissue-Tek OCT compound (Sakura Finetek, Torrance, CA, USA) in liquid nitrogen and stored at −80°C. The CB tissues were then sectioned into 16 μm sections using a cryostat (Leica Microsystems, Wetzlar, Germany) and mounted on Superfrost Plus slides (VWR International Ltd, Lutterworth, UK). The slides were allowed to dry before storing at −80°C.

Isolation of single cells

The carotid artery bifurcations were quickly dissected out from anaesthetized mice and kept in ice-cold phosphate-buffered saline (PBS). The superior cervical ganglion was carefully removed from the bifurcation, and the CB was gently teased free from the surrounding tissue in the bifurcation. The CB was later transferred to enzyme digestion solution containing 0.1% trypsin and 0.1% collagenase in PBS. The tissue was digested for 15 min on a 37°C shaker at 60 rpm. Minimal Essential Medium (Gibco, Gaithersburg, MD, USA) containing 10% fetal bovine serum was quickly added to stop the enzyme reaction. The CBs were gently triturated using a heat-polished Pasteur pipette previously coated with 0.1% BSA-PBS. The cells were then centrifuged at 1000 rpm for 5 min and resuspended in 0.1% BSA-PBS. The cells were subsequently placed in a 60 mm Petri dish containing 0.1% BSA-PBS for observation. A single cell was picked with a microcapillary and placed in another Petri dish with 0.1% BSA-PBS to confirm that only one cell was picked. Once confirmed, the cell was picked again and seeded into a PCR tube containing ice-cold cell lysis mix. For each isolation experiment, 19 or 39 cells were picked. For OSN or vomeronasal sensory neuron (VSN) dissociation, a similar protocol was used, except that the enzyme digestion solution contained a final concentration of 0.1% collagenase and 0.2% dispase.

Single cell RT-PCR

For each single cell RT-PCR experiment, PCR tubes with ice-cold cell lysis mix containing PCR buffer (Roche, Basel, Switzerland), NP-40 (Roche), $MgCl_2$ (Roche), DTT (Invitrogen, Carlsbad, CA, USA), RNase inhibitors mix [RNase inhibitor (Qiagen, Valencia, CA, USA) and RNasin (Promega)], Anchor T primers (Integrated DNA Technologies, Coralville, IA, USA) and dNTPs (Takara Bio Inc., Otsu, Japan) were prepared. Cells were heated to 65°C for 1 min to promote unfolding of RNAs and quickly chilled on ice afterwards. Then RT mix containing Superscript II (Invitrogen), RNase inhibitors mix (RNase inhibitor and RNasin) and T4 gene 32 (Roche) was added. For each round of experiment, two negative controls were included: one without any cell, and one without any reverse transcriptase. The RNAs were then incubated at 37°C for 10 min to generate cDNAs. The cDNAs were then treated with Exonuclease I (New England Biolabs, Beverly, MA, USA) to remove redundant primers and further incubated with TdT (Roche) and RNaseH (Roche) for the addition of poly(A) tails. For the final PCR step, the RT tailed products were amplified with Anchor T primers and subsequently run in agarose gels to check for appropriate DNA products.

Marker genes analysis for identifying candidate cells of interest

Each single cell-derived cDNA was diluted and used as a template for PCR amplification of published CB glomus cell markers: tyrosine hydroxylase (Th), ubiquitin carboxy-terminal hydrolase L1 (Uchl1, also known as PGP9.5), potassium channel subfamily K member 3 (Kcnk3, also known as TASK1). Single cells capable of amplifying all these marker genes were considered candidate CB glomus cells. The remaining RT tailed products from the candidate cell were used to generate additional cDNAs according to the protocol described above. For the identification of candidate OSNs or VSNs, a similar protocol was used except for the marker genes amplified. OSN markers include the olfactory marker protein (Omp); guanine nucleotide binding protein, α stimulating, olfactory type (Gnal); cyclic nucleotide gated channel α 2 (Cnga2); and adenylate cyclase type 3 (Adcy3). VSN markers include guanine nucleotide binding protein, α O (Gnao1); guanine nucleotide binding protein, α inhibiting 2 (Gnai2); olfactory marker protein (Omp); transient receptor potential cation channel subfamily C member 2 (Trpc2); calreticulin 4 (Calr4); and β-2 microglobulin (B2m).

Illumina sequencing library preparation

We selected the amplified cDNAs of eight candidate CB glomus cells, two candidate OSNs and two candidate VSNs for the construction of Illumina sequencing libraries. For glomus cell 1, the cDNAs were gel-purified and sheared using Covaris S220 Focused-ultrasonicator (Woburn, MA, USA). DNAs in the 150–300 bp ranges were purified and sequencing adaptors (Illumina, Inc., San Diego, CA, USA) were added in accordance with the manufacturer's instructions. The library was then subjected to 36-bp single-end sequencing on the Illumina GA2000 system. For the remaining samples, the cDNAs were gel-purified or bead-purified (Agencourt AMPure XP; Beckman Coulter, Fullerton, CA, USA) and tagmentated using the Nextera DNA sample preparation kits (Illumina Inc.)

in accordance with the manufacturer's instructions. The libraries were then multiplexed and sequenced using the Illumina HiSeq system with a 50-bp length.

Sequencing analysis

FASTQ files from the sequencing runs were aligned to the mouse reference genome (mm10) using Bowtie –m 1 option to obtain uniquely mapped reads. Output SAM-files were summarized and subjected to gene annotation using ANNOVAR (Wang *et al.* 2010). Reads aligned to exonic regions of the RefGene were counted and the relative gene expression levels were summarized as RPM values (the number of reads mapped to each gene per million of total mapped reads). Because reverse transcription was limited to 10 min, the sizes of cDNAs were similar (0.5∼1.5 kb in length). Hence, transcript lengths were not considered in the normalization. Genes with multiple transcript variants were combined into one count. The expression profiles of CB glomus cells were submitted to NCBI Gene Expression Omnibus (GEO) database (GEO ID: GSE76579).

In situ hybridization

CB tissue sections (16 μm) were fixed in 4% paraformaldehyde (PFA) for 15 min. The slides were washed with PBS, followed by an acetylation step with acetic anhydride in triethanolamine solution. Next, the slides were washed with PBS and then incubated with hybridization buffer for at least 1 h at 58°C to prevent non-specific binding. Following prehybridization, hybridization buffer containing digoxigenin (DIG)-labelled antisense RNA probes was added to each slide and allowed to incubate at 58°C overnight. DIG-labelled antisense RNA probes were generated from cDNA fragments using the DIG RNA labelling mix (Roche) and T3 RNA polymerase (Promega). After multiple washes in saline sodium citrate, the slides were incubated in 0.5% Blocking Reagent (Roche) in PBS for at least 30 min before incubation in 1:5000 anti-DIG-AP antibody in blocking solution. The slides were washed with PBS before an overnight incubation in 5-bromo-4-chloro-3-indolyl phosphate/nitro blue tetrazolium that helped visualize the hybridized mRNAs. The slides were subsequently mounted with Mowiol (Kuraray Europe GmbH, Hattersheim am Main, Germany). Digital images of the CB regions were obtained with a camera (Qimaging, Surrey, BC, Canada) on an inverted microscope (Carl Zeiss, Oberkochen, Germany) and analysed using ImageJ (NIH Bethesda, MD, USA). The region containing the CB was selected and the ImageJ default colour thresholder was used to differentiate CB glomus cells regions and the background region. Mean pixel intensity was calculated for each region, and the relative intensity of CB glomus cell signal was calculated by dividing background pixel intensity by CB glomus cell pixel intensity.

Immunohistochemistry

CB tissue sections (16 μm) were fixed in 4% PFA for 15 min and permeabilized for 1 min in 0.5% Triton X-PBS. Briefly after PBS rinses, the slides were blocked with 5% skim milk in 0.1% Triton X-PBS for at least 30 min. Afterwards, primary antibodies diluted in the same blocking solution were added onto the slides for an overnight incubation at 4°C. Following multiple PBS washes, the slides were incubated with the appropriate secondary antibody along with nuclear Hoechst stain (bisBenzimide, B2883; Sigma-Aldrich, St Louis, MO, USA). The slides were washed and mounted with Mowiol. Digital images of the CB regions were obtained with a QImaging camera on a Zeiss inverted microscope. Rabbit anti-Th (AB152, Millipore, Billerica, MA, USA; dilution 1:1000); rabbit anti-Ndufa4l2 (16480-1-AP, Proteintech, Chicago, IL, USA; dilution 1:1000); rabbit anti-Syp (SAB4502906, Sigma-Aldrich; dilution 1;100); Goat anti-Gnas (SAB2501411, Sigma-Aldrich; dilution 1:100); donkey anti-rabbit Cy3 (Jackson ImmunoResearch, West Grove, PA, USA; dilution 1:200); and donkey anti-goat Cy3 (Jackson ImmunoResearch; dilution 1:100).

Cloning

Approximately 400 bp sequences in the 3′ UTR or the open reading frame were amplified from the cDNAs of C57BL/6 mouse CB and brain. For olfactory receptor Olfr78, the entire open reading frame was amplified. The sequences were subcloned into pCI expression vectors (Promega) and verified by Sanger sequencing (3100 Genetic Analyser; Applied Biosystems, Foster City, CA, USA).

LacZ staining

Freshly dissected carotid artery bifurcations from heterozygous Olfr78^{tm1Mom}/MomJ mice were fixed in 4% PFA for 15 min followed by three 5-min PBS washes. The tissues were then incubated in X-gal Reaction Buffer (Zymo Research, Irvine, CA, USA) for 3 h at 37°C and washed with PBS before viewing under bright field optics.

Luciferase assay

The Dual-Glo Luciferase Assay System (Promega) was used to measure receptor responses as described previously (Zhuang & Matsunami, 2008). HEK293T cells were transfected with 5 ng well^{-1} of pRL-SV40, 10 ng well^{-1} of luciferase driven by a cAMP response element and 5 ng well^{-1} of plasmids encoding Olfr78. Odourant stocks (1 M) were diluted in DMSO. Twenty-four hours

after transfection, transfection medium was removed and replaced with CD293 medium (Gibco) containing the appropriate concentration of odourants diluted from the 1 M stocks. Four hours after the odour stimulation, luminescence was measured using a Polarstar Optima plate reader (BMG Labtech, Ortenberg, Germany). All luciferase luminescence values were divided by the Renilla luciferase values to obtain normalized responses and control for transfection efficiency.

Screening procedure

We stimulated the olfactory receptor Olfr78 with 345 odourants at 300 μM in duplicates and ranked the top 20 odourant-receptor pairs by their Luc/RL ratios (the cAMP driven luciferase value divided by the Renilla luciferase value). We then performed a secondary screening where Olfr78 was tested against a no-odour control as well as 3, 30 and 300 μM of each of the 20 agonists identified in the primary screening. Each comparison was performed in triplicates. The final dose–response curves were generated for sodium acetate (pH 7.4) and acetic acid against ten concentrations in quadruplicate.

Statistical analysis

Pearson correlation coefficients between different RNA-Seq experiments were computed using relative expression levels (RPM) in Stata (StataCorp, College Station, TX, USA) and Prism, version 6 (GraphPad Software Inc., San Diego, CA, USA). To calculate correlation coefficients between RNA-Seq data and microarray data, relative rankings based on gene expression levels were compared. Principal component analysis was performed after normalizing the read counts from all expressed genes across 12 single cells using the DESeq package (Anders & Huber, 2010). For the differential expression analysis, we compared CB glomus cells with 17 non-CB tissues using the edgeR package (Robinson & Smyth, 2008; Robinson *et al.* 2010). Non-CB tissues included our OSN and VSN RNA-Seq data, as well as 15 other mouse tissues downloaded from GSE29184 (Shen *et al.* 2012). The raw sequences from different tissue RNA-Seq were processed through the same pipeline used for the single-cell data to obtain read counts. By using the default edgeR setting, we used the read counts and treated them as two groups (CB and non-CB group) and as our single factor for the software to apply model-based normalization. In this case, the quantile-adjusted conditional maximum likelihood method was used to calculate the likelihood by conditioning on the total counts for each gene and pseudo counts were used after adjusting the library sizes. The pseudo counts could be viewed as normalized counts. Overall, to search for the CB-specific genes, we were only concerned with the differential expression between groups rather than the quantification of gene expression; therefore, no additional normalization was applied to both single cell and tissue data. CB-specific genes were defined as having P values below 0.01 after correcting for false discovery rates. To generate heat maps for the top differentially expressed genes, relative rankings based on gene expression levels were calculated for all expressed genes in each tissue. The most weakly expressed gene is ranked at 100% along with other non-expressed genes.

For the primary screening for Olfr78 ligands, the Z-score was used to rank odour-receptor pairs. For the secondary screening for Olfr78, a two-sided Student's t test was used to compare stimulated wells and no odour control wells in triplicates. For ligands with $P < 0.05$, dose–response curves were generated. The dose–response curves report the mean $\pm$ SEM from quadruplicates. The data were fitted with a three-parameter logistic model. Data were analysed with Excel (Microsoft Corp., Redmond, WA, USA) and Prism, version 6 (GraphPad).

Results

Evaluating the single cell RNA-Seq approach

To obtain the gene expression profile of CB glomus cells using the single cell RNA-Seq approach (Fig. 1), we first aimed to evaluate our technique using a well-characterized chemosensory cell, the OSN, for which the canonical signal transduction components have been fully identified and conventional RNA-Seq data are available.

Two OSNs were selected to generate independent single cell-derived cDNA libraries that yielded an average of 5 million reads (Table 1), comparable to other whole tissue RNA-Seq results. The majority of the reads (78.83%) mapped to the mouse reference genome (mm10) and only reads with a single alignment to the exonic regions were counted. Comparison of gene expression levels between these individual single OSNs showed strong correlation (Pearson correlation of 0.82) (Fig. 2*A*), with increased variation occurring in genes with medium to low expression, as previously shown in other single cell RNA-Seq studies (Wu *et al.* 2014). Consistent with the current knowledge, each OSN expressed one major unique olfactory receptor at a high level, highlighting a true transcriptome difference between the two samples. To examine whether our single OSN expression profiles agree with that of conventional RNA-Seq, we compared the average relative gene expression of two single OSNs with published RNA-Seq data from fluorescence-activated cell sorted mature OSNs (Magklara *et al.* 2011). Indeed, we observed a positive correlation (Pearson correlation of 0.68) (Fig. 2*B*). Notably, all the known genes encoding the canonical signal transduction components in OSNs were highly expressed, including Gnal (guanine nucleotide

binding protein, α stimulating, olfactory type), Cnga2 (cyclic nucleotide gated channel α 2) and Adcy3 (adenylyl cyclase type 3). In addition, known olfactory markers, including Omp (olfactory marker protein) and Rtp1 (receptor-transporting protein 1), were also among the most abundant transcripts.

Taken together, our data suggest that abundantly expressed genes can be identified via the single cell RNA-Seq approach, which can serve as a powerful tool to screen for key transcripts expressed in rare cell types.

Transcriptome analysis of single CB glomus cells

We next applied our single cell RNA-Seq method to CB glomus cells. We dissociated tissues containing the CB, picked single cells and amplified cDNAs derived from each single cell. To select cDNA samples derived from CB glomus cells, we conducted marker genes analysis. Each single cell-derived cDNA sample was used as a template for PCR diagnosis with primers complementary to three glomus cell markers (Th, tyrosine hydroxylase; Uchl1, ubiquitin carboxyl-terminal esterase L1, also known as PGP9.5; Kcnk3, potassium channel subfamily K member 3, also known as TASK1), as well as a housekeeping gene Gapdh. Single cells positive for all glomus cell markers tested were considered as candidate CB glomus cells (Fig. 3*A*).

Illumina sequencing libraries for eight candidate CB glomus cells were constructed and sequenced (Table 1). The eight CB glomus cells generated an average of 39 million reads, with an average of 88.81% of the reads mapped to the reference mouse genome (mm10). The number of genes detected in each cell ranged from 5007 to 7742, which is consistent with other single cell transcriptome studies (Ramskold *et al.* 2012; Hanchate *et al.* 2015). Their read distributions followed a similar pattern among the eight samples (Fig. 3*B*). Similar to other single-cell RNA-Seq studies (Shalek *et al.* 2013; Jaitin *et al.* 2014; Patel *et al.* 2014), the transcriptomes of separately processed single CB glomus cells correlated well with each other, yet demonstrated individual variation (mean Pearson correlation: 0.63, $0.32 < r < 0.84$) (Fig. 3*C*). When the average expression profile of these single CB glomus cells was compared with published whole CB RNA-Seq and microarray data (Balbir *et al.* 2007; Chang *et al.* 2015), we also saw positive correlations (Pearson correlation of 0.58 and 0.59) (Fig. 3*D* and *E*). As expected, the top 1% genes from our single CB glomus cells occupied high rankings in the whole CB data, albeit lower than they were in CB glomus cells. For these genes, an average ranking of top 5% was observed in the C57BL/6J CB RNA-Seq data, and their average ranking was in the top 10% of the DBA/2J CB microarray data. Intriguingly, the top 1% genes from the whole CB data were not highly ranked in our CB glomus cells, with an average ranking of 28% and 46%, respectively, for the C57BL/6J RNA-Seq and the DBA/2J microarray, probably reflecting the fact that the fraction of glomus cells in the whole CB is relatively low. These suggest that our single cell RNA-Seq data vastly enriched for glomus cell specific transcripts. The most highly expressed genes uncovered through our single CB glomus cell RNA-Seq are listed in Table 2, many of which have not been previously reported in CB glomus cells.

Validation of single CB glomus cell RNA-Seq

Although our single cell RNA-Seq experiments generated a comprehensive transcriptome profile, it is difficult to

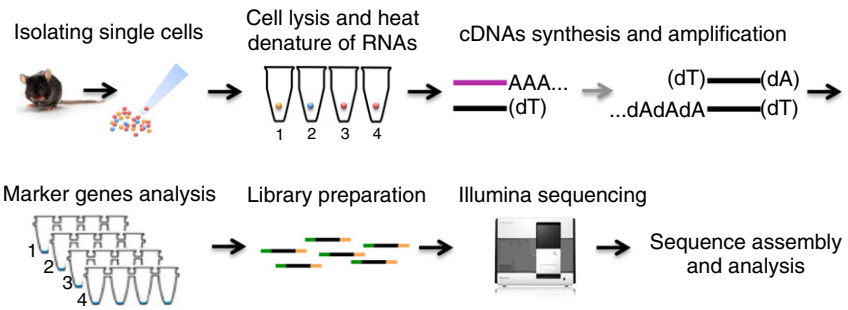

Figure 1. Workflow of preparing single cell RNA-Seq
The tissue of interest was dissected out from mice for further enzymatic and mechanical treatment to obtain single cells in suspension. Cells are coloured differently to represent the heterogeneity of cell types present at this step. Each individual single cell was carefully dispensed into a PCR tube containing lysis buffer and heated for RNA denaturation. mRNAs were reverse transcribed using anchor T primers and further processed to generate poly(A) tailed single-stranded cDNAs, which were subsequently amplified using anchor T primers. To identify the cell type of interest, each single cell-derived cDNA was used as a template for the marker genes analysis. cDNAs capable of amplifying specific cell type markers were selected and used for Illumina library preparation and sequencing. Sequences from these candidate cells were then aligned to the current mouse genome database for further analysis.

Table 1. Summary of single cell RNA-Seq details

Cell	Mouse strain	Illumina platform	Read length	Reads with one alignment	Reads with multiple alignments	Reads with no alignment	Total reads
OSN1	C57BL/6J × CAST/EiJ	HiSeq	50 bp	3,431,160 (61.23%)	769,494 (13.73%)	1,402,698 (25.03%)	5,603,352
OSN2	C57BL/6J × CAST/EiJ	HiSeq	50 bp	4,076,868 (66.81%)	968,909 (15.88%)	1,055,971 (17.31%)	6,101,748
Glomus cell 1	C57BL/6J	GA2000	36 bp	5,709,578 (58.76%)	1,951,978 (20.09%)	2,055,039 (21.15%)	9,716,595
Glomus cell 2	C57BL/6J × SPRET/EiJ	HiSeq	50 bp	113,034,997 (69.40%)	32,543,457 (19.98%)	17,299,429 (10.62%)	162,877,883
Glomus cell 3	C57BL/6J	HiSeq	50 bp	15,045,753 (67.65%)	4,710,465 (21.18%)	2,485,967 (11.18%)	22,242,185
Glomus cell 4	C57BL/6J	HiSeq	50 bp	14,936,522 (68.80%)	4,945,355 (22.78%)	1,828,792 (8.42%)	21,710,669
Glomus cell 5	C57BL/6J	HiSeq	50 bp	12,422,108 (69.31%)	3,670,097 (20.48%)	1,830,883 (10.22%)	17,923,088
Glomus cell 6	C57BL/6J	HiSeq	50 bp	22,711,176 (70.98%)	6,242,775 (19.51%)	3,043,914 (9.51%)	31,997,865
Glomus cell 7	C57BL/6J	HiSeq	50 bp	16,018,321 (66.74%)	5,840,606 (24.34%)	2,141,508 (8.92%)	24,000,435
Glomus cell 8	C57BL/6J	HiSeq	50 bp	18,546,167 (68.14%)	6,077,140 (22.33%)	2,595,193 (9.53%)	27,218,500

exclude the possibility that contamination of non-glomus cells affected the RNA-Seq data relying solely on sequencing analysis. To confirm which genes were expressed in the CB glomus cells *in vivo*, we conducted *in situ* hybridizations for 53 selected genes using acutely frozen carotid arteries containing CB and surrounding tissues from mice 3 weeks or older. We did not limit our selection to the most highly ranked genes but included 17 genes that ranked among the top 30, 13 genes that ranked between 31st to 300th, and 22 genes that ranked

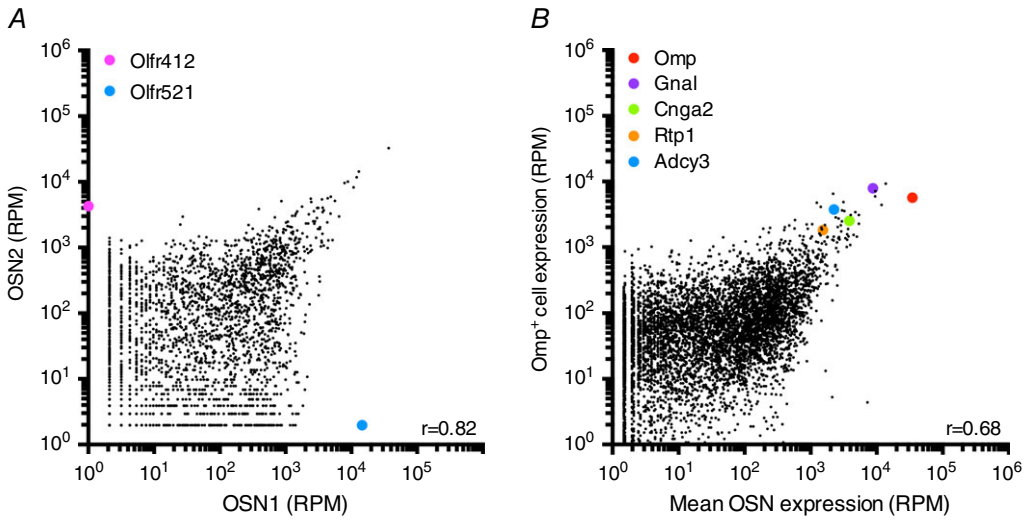

Figure 2. Transcriptome comparison of single OSNs
A, scatter plot of gene expression profiles (RPM values) from individually picked and processed single OSNs. The Pearson correlation coefficient between the two samples is indicated. Coloured dots represent the predominant olfactory receptor expressed in each OSN. *B*, scatter plot comparing the average expression profile of our single OSNs with the transcriptome of fluorescence-activated cell sorted mature OSNs (Omp positive cells). The Pearson correlation coefficient is indicated. Coloured dots label genes crucial to OSN function. Omp, olfactory marker protein; Gnal, guanine nucleotide binding protein, α stimulating, olfactory type; Cnga2, cyclic nucleotide gated channel α2; Rtp1, receptor transport protein 1; Adcy3, adenylate cyclase type 3.

between 300th to 7000th, as well as Olfr558, a gene not detectable in our sequencing results. As expected, Olfr558 did not show obvious signals (Fig. 4*A*), and the quantification of relative staining intensity showed that it had the least hybridization signal among all 53 probes tested. Similar to the staining pattern using the glomus cell marker Th (Fig. 4*D*), 40 probes marked the clustered glomus cells typical of CB glomeruli (Fig. 4*A*–*E*), which mostly covered genes encoding the GPCR signalling pathway (Fig. 4*A*), ion channels and associated proteins (Fig. 4*B*), the HIF pathway (Fig. 4*C*), and neuronal markers (Fig. 4*D*). For a set of candidate genes including Gnas, Ndufa4l2, Syp and Th, protein expression was additionally confirmed via immunohistochemistry (Fig. 4*F*). Taken together, our single cell RNA-Seq data indeed derived from CB glomus cells and represent their transcriptome.

Comparison of CB glomus cells with other cell types

How unique is the CB glomus cell transcriptome? We first compared gene expression profiles between single CB glomus cells and single OSNs or single VSNs, another class of chemoreceptors that we had sequenced. The Pearson correlation coefficients between the CB glomus cell and the OSN/VSN were as low as 0.12 and 0.20 (Fig. 5*A* and *B*), indicative of marked differences in transcriptomes among the three cell types. When principal component analysis was performed for the expression profiles of these 12 cells, discrete separations among each cell type were observed (Fig. 5*C*). Taken together, our data suggest unique transcriptome profiles in each of the chemosensory cells.

We next explored which genes were uniquely expressed in the CB glomus cells. Differential gene expression

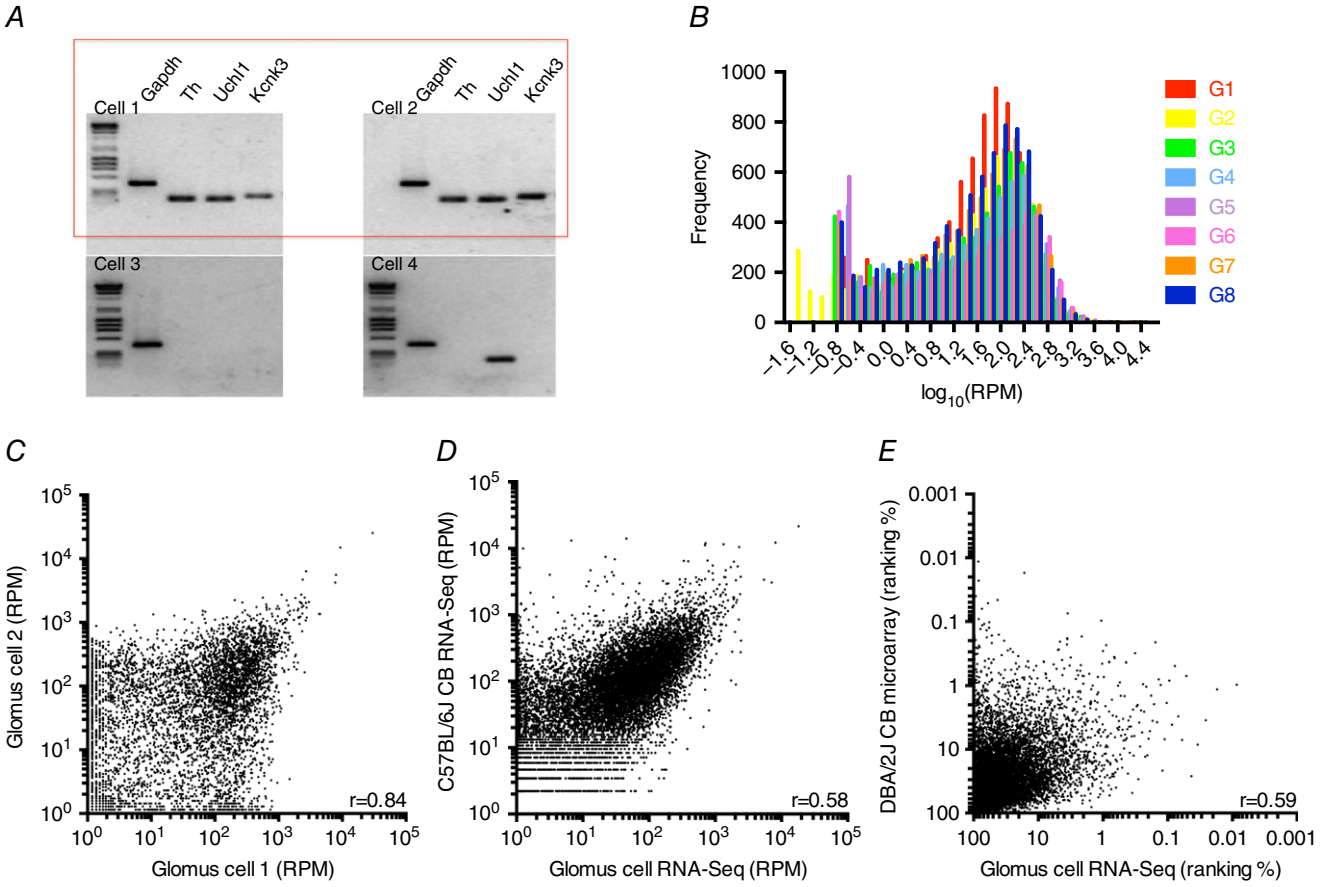

Figure 3. Transcriptome comparison of single CB glomus cells
A, representative marker genes analysis for four single cells isolated from CB dissociations. Cells 1 and 2 are considered candidate CB glomus cells as a result of their expression of glomus cell markers Th (tyrosine hydroxylase), Uchl1 (ubiquitin carboxy-terminal hydrolase L1) and Kcnk3 (potassium channel subfamily K member 3). *B*, histogram of the RPM values of all detected genes in eight individually picked and processed candidate CB glomus cells (G1 through G8). *C*, scatter plot of gene expression profiles (RPM values) from two single CB glomus cells. The Pearson correlation coefficient between the two samples is indicated. *D*, scatter plot of mean expression profiles from single CB glomus cell RNA-Seq and C57Bl6/J CB RNA-Seq. The Pearson correlation coefficient is indicated. *E*, scatter plot of mean expression profiles from single CB glomus cell RNA-Seq and DBA/2J CB microarray. Mean expression levels were calculated and their relative rankings were used for comparison. The Pearson correlation coefficient is indicated.

Table 2. Top 15 most abundant genes in CB glomus cells

Rank	Gene symbol	Gene name	Average expression (RPM)
1	Gnas	GNAS (guanine nucleotide binding protein, α stimulating) complex locus	18,169
2	Epas1 (Hif2a)	Endothelial PAS domain-containing protein 1	8096
3	Rgs4	Regulator of G-protein signalling 4	7141
4	Ndufa4l2	NADH dehydrogenase [ubiquinone] 1α subcomplex subunit 4-like 2	5456
5	Nnat	Neuronatin	2451
6	Cyb561	Cytochrome b-561	2422
7	Eml5	Echinoderm microtubule-associated protein-like 5	2412
8	Pkib	cAMP-dependent protein kinase inhibitor β	2371
9	Itm2b	Integral membrane protein 2B	2298
10	Snap25	Synaptosomal-associated protein 25	2267
11	Ddc	Dopa decarboxylase	2183
12	Slc39a6	Zinc transporter ZIP6 precursor	2130
13	Olfr78	Olfactory receptor 78	2078
14	Dgkk	Diacylglycerol kinase kappa	2048
15	Th	Tyrosine hydroxylase	2043

Average relative gene expression in CB glomus cells was calculated from eight separately prepared single glomus cell RNA-Seq datasets.

analysis was conducted between CB glomus cells and 15 other mouse tissues (Shen *et al.* 2012), as well as single cell RNA-Seq data of the OSN and the VSN. Overall, 7110 genes were differentially expressed with $P < 0.01$ after correcting for false discovery rates, among which 448 were over-represented and 6662 were under-represented in CB glomus cells (Fig. 6*A*). Overall, the majority of these differentially expressed CB glomus cell genes display substantial expression level differences compared to the RNA-Seq data of other non-CB tissues (Fig. 6*B*). The drastic differences displayed here further suggest that the CB glomus cell is a distinct sensory cell type, consistent with its unique function.

GPCR signalling components are abundantly expressed in CB glomus cells

A prominent feature of the CB transcriptome profile is the enrichment of various guanine nucleotide-binding proteins (G proteins) that constitute the heterotrimeric G protein complex, an important component of the GPCR signalling pathway (Table 3). The α subunits of several G protein families were detected at high levels. In particular, the most abundant transcript in glomus cells was stimulatory G protein α (Gnas, also known as $G_{\alpha s}$), representing 1.82% of the total transcripts. mRNA and protein expression for this cAMP pathway-activating molecule was confirmed by *in situ* hybridization and immunohistochemistry (Fig. 4*A* and *F*). G protein α olfactory type (Gnal, also known as $G_{\alpha olf}$), which is functionally similar to $G_{\alpha s}$, was also detected. Other highly expressed G protein α subunits include the cAMP-inhibiting G protein α i2/i3 (Gnai2, Gnai3) and G protein α O (Gnao1), as well as the phospholipase C-activating G protein α q and 11 (Gnaq, Gna11). In line with this, β and γ subunits of the heterotrimeric G protein complexes were also abundantly expressed, such as Gnb1, Gnb2, Gng2, Gng3, Gng10 and Gng12.

Consistent with the abundant expression of G proteins, several GPCRs were detected at high levels (Table 4). Notably, the olfactory receptor Olfr78 that couples to $G_{\alpha s/olf}$ was found to be the most abundant GPCR in the CB glomus cell transcriptome, consistent with the recent finding that Olfr78 is highly enriched in mouse CB (Chang *et al.* 2015). Other highly expressed GPCRs detected include previously reported adenosine receptor (Adora2a), purinergic receptor (P2ry12), cannabinoid receptor (Cnr1) and pituitary adenylate cyclase-activating polypeptide (PACAP) receptor (Adcyap1r1) (Conde & Monteiro, 2004; McLemore *et al.* 2004; Xu *et al.* 2005; Conde *et al.* 2006; Lam *et al.* 2012), as well as two unreported GPCRs, latrophilin receptor (Lphn1) and Leucine-rich repeat-containing GPCR (Lgr5). The list of GPCRs with less abundant sequencing reads in our single cell RNA-Seq (genes ranked blow the top 10%) also included previously identified CB GPCRs, such as type-1A angiotensin II receptor (Agtr1a), dopamine receptor (Drd2) and endothelin-1 receptor (Ednra) (Gauda *et al.* 1996; Fung *et al.* 2001; Chen *et al.* 2002). The various ligands activating these receptors suggest their potential influence over CB sensory activities.

Among the highly expressed GPCR signalling genes in CB glomus cells, more than half of them are involved in the cAMP-mediated GPCR signalling pathway (Table 5). Molecules participating in this pathway include $G_{\alpha s}$-coupled GPCRs (Olfr78, Adora2a, Adcyap1r1), $G_{\alpha i}$-coupled GPCRs (P2ry12, Cnr1), G proteins that regulate adenyl cyclase (Gnas, Gnao1, Gnai2, Gnai3,

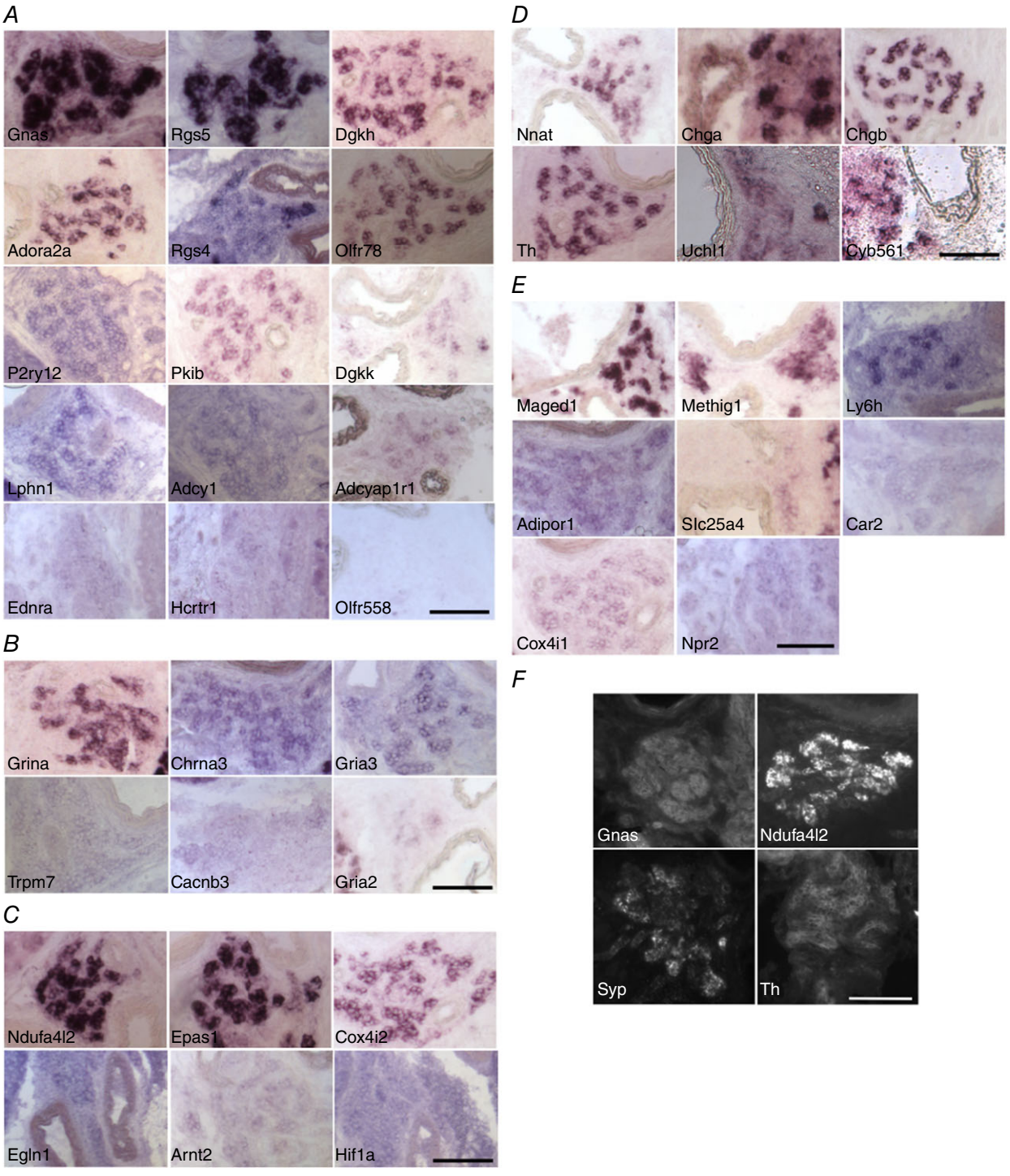

Figure 4. Validation of single CB glomus cell RNA-Seq data using *in situ* hybridization and immunohistochemistry
A–E, genes identified through single CB glomus cell RNA-Seq were confirmed by *in situ* hybridization. CB sections from mice 3 weeks or older were hybridized with DIG-labelled antisense RNA probes of GPCR signalling components (*A*), ion channels and associated proteins (*B*), HIF pathway components (*C*), neuronal markers (*D*) and others (*E*). Olfr588, not detected in CB glomus cell RNA-Seq, served as a negative control (*A*). Scale bar = 100 μm. *F*, representative images of adult mouse CB sections stained with primary antibodies specific for the proteins of several highly abundant genes identified in the single CB glomus cell RNA-Seq. Scale bar = 100 μm. Gnas, (guanine nucleotide binding protein, α stimulating) complex locus; Rgs5, regulator of G-protein signalling 5; Dgkh, diacylglycerol kinase eta; Adora2a, adenosine receptor A2a; Rgs4, regulator of

Gnal), the cAMP-activating adenyl cyclase (Adcy1), the cAMP-dependent protein kinase A (PKA) (Prkar1a, Prkacb, Prkaca, Prkar2a) and PKA regulators (Pkib, Akap9, Akap11, Akap8). Also notable was the presence of the protein kinase C (PKC)-mediated GPCR signalling pathway components (Table 5). This is supported by the expression of $G_{\alpha q/11}$-coupled GPCRs (Agtr1a, and Ednra) and corresponding G proteins (Gnaq, Gna11), downstream effectors such as PKC (Prkce, Prkca), as well as several diacylglycerol (DAG) kinases (Dgkk, Dgkh, Dgkg). Moreover, we noted some highly ranked genes that undertake roles in regulating GPCR signalling (Table 5), such as regulators of G protein signalling family members (Rgs4, Rgs5) that facilitate the hydrolysis of GTP-bound G proteins.

Taken together, the abundant GPCR signalling pathway transcripts detected in CB glomus cells emphasize the notion that GPCR signalling, especially the cAMP-mediated signal transduction pathway, is important in modulating CB function. Furthermore, we have characterized several GPCRs and GPCR signalling components not previously described in CB glomus cells.

High-throughput heterologous screening identifies acetate as a CB GPCR ligand

According to our RNA-Seq data, olfactory receptor Olfr78 was the most abundant GPCR in CB glomus cells. Olfr78 is a relatively conserved olfactory receptor, with conserved orthologues found in mammals and birds (Fig. 7*A*). Interestingly, the intact Olfr78 sequence is also present in dolphins, a species without an olfactory nerve, suggesting an ectopic functional significance outside of olfaction. To validate active Olfr78 expression in the CB *in vivo*, we performed lacZ staining using an Olfr78-IRES-taulacZ transgenic mouse strain Olfr78^{tm1Mom}/MomJ, where the Olfr78 coding sequence is replaced with GFP followed by IRES-taulacZ (Bozza *et al.* 2009). As shown in Fig. 7*B*, blue precipitations marked the cells in the CB but not any other cells in the nearby superior cervical ganglion, indicative of an active Olfr78 promoter in CB glomus cells. GPCRs expressed in CB glomus cells, such as the adenosine receptor and the PACAP receptor, have been shown to affect CB sensory activities through receptor activation. Analogous to this, ligands for Olfr78 can probably also affect CB function. To identify such ligands, we utilized an established heterologous cell system for screening olfactory receptors (Zhuang & Matsunami, 2008). Olfr78 was expressed in HEK293T cells and cAMP-induced luciferase activity was monitored after exposure to different chemicals. A screening was performed on Olfr78 against 345 diverse odourants. After a secondary screening, we found that two short chain fatty acids (SCFA), acetic acid and propionic acid, act as potent Olfr78 agonists, whereas some other SCFA, such as lactic acid, mildly activated Olfr78 (Fig. 7*C*), consistent with previous studies (Saito *et al.* 2009; Pluznick *et al.* 2013; Chang *et al.* 2015). We further showed that Olfr78 responded similarly to both acetic acid and sodium acetate (pH 7.4) (EC_{50} = 0.5 mM), suggesting that acetate, not acid, is activating this receptor (Fig. 7*D*). In summary, we identified the SCFA-sensing olfactory receptor in the CB glomus cells that may contribute to chemosensory function in the CB.

CB glomus cells express various types of ion channels

The signal transductions of CB glomus cells rely on modulation of channel opening probabilities, a process that is not fully understood. To help address this question, we compiled a list of abundant ion channels identified through the single CB glomus cell RNA-Seq (Table 6). Ion channels from a variety of families were detected in CB glomus cells, many of which were expressed at moderate levels, yet still confirmed previous studies (Table 7).

Consistent with a prominent role of the background potassium channels in initiating glomus cell depolarization under hypoxia (Buckler *et al.* 2000; Buckler, 2007),

G-protein signalling 4; Olfr78, olfactory receptor 78; P2ry12, P2Y purinoceptor 12; Pkib, cAMP-dependent protein kinase inhibitor β; Dgkk, diacylglycerol kinase kappa; Lphn1, latrophilin-1 precursor; Adcy1, adenylate cyclase type 1; Adcyap1r1, pituitary adenylate cyclase-activating polypeptide type I receptor; Ednra, endothelin-1 receptor precursor; Hcrtr1, orexin receptor type 1; Olfr558, olfactory receptor 558; Grina, glutamate receptor, ionotropic, *N*-methyl-D-aspartate-associated protein 1; Chrna3, neuronal ACh receptor subunit α-3 precursor; Gria3, glutamate receptor 3; Trpm7, transient receptor potential cation channel subfamily M member 7; Cacnb3, voltage-gated L-type calcium channel subunit β-3; Gria2, glutamate receptor 2; Ndufa4l2, NADH dehydrogenase [ubiquinone] 1α subcomplex subunit 4-like 2; Epas1, endothelial PAS domain-containing protein 1; Cox4i2, cytochrome *c* oxidase subunit 4 isoform 2; Egln1, egl-9 family hypoxia-inducible factor 1; Arnt2, aryl hydrocarbon receptor nuclear translocator 2; Hif1α, hypoxia-inducible factor 1-α; Nnat, neuronatin; Chga, chromogranin a; Chgb, chromogranin b; Th, tyrosine hydroxylase; Uchl1, ubiquitin carboxy-terminal hydrolase L1; Cyb561, cytochrome b561; Maged1, melanoma-associated antigen D1; Methig1, methyltransferase hypoxia inducible domain containing 1; Ly6h, lymphocyte antigen 6 complex, locus H; Adipor1, adiponectin receptor 1; Slc25a4, solute carrier family 25 (mitochondrial carrier, adenine nucleotide translocator), member 4; Car2, carbonic anhydrase 2; Cox4i1, cytochrome *c* oxidase subunit 4 isoform 1; Npr2, atrial natriuretic peptide receptor 2 precursor; Syp, synaptophysin.

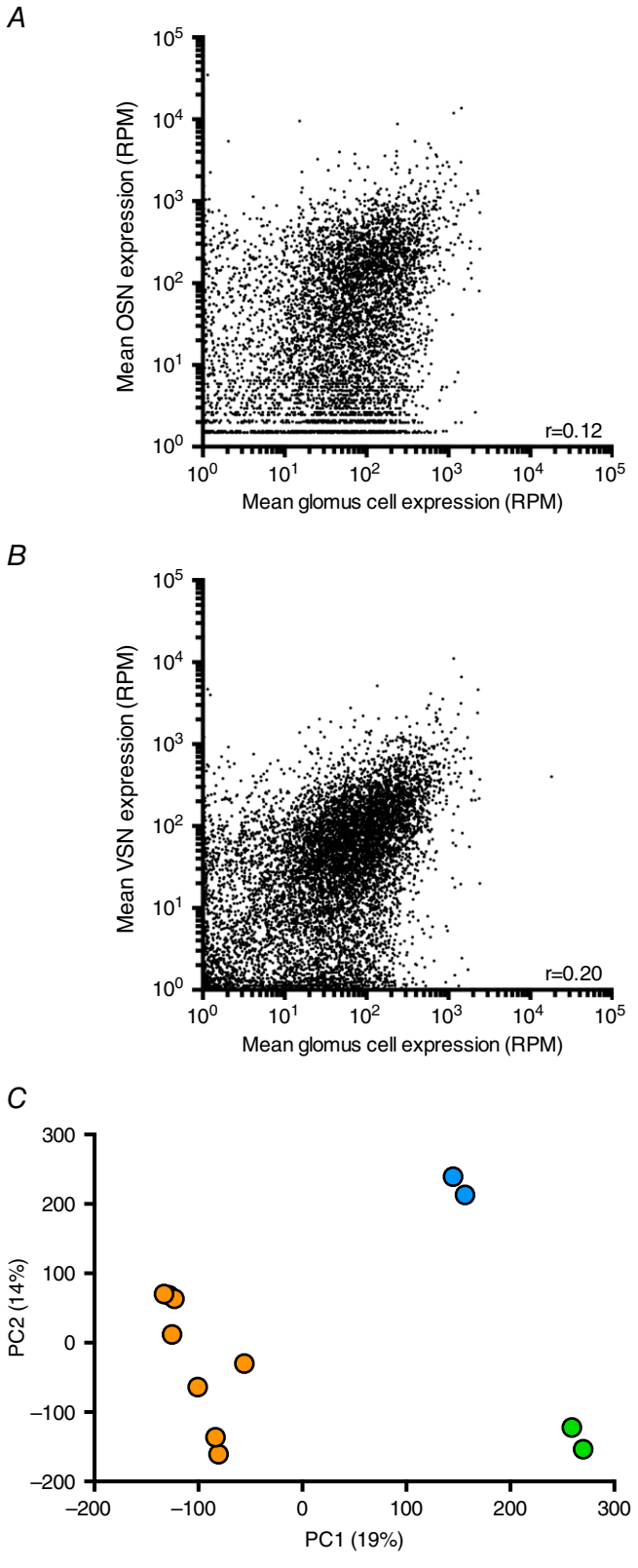

Figure 5. Transcriptome comparison between single CB glomus cells and other cell types
For each cell type, the average RPM values are the mean expression levels from separately picked and processed single cells. *A*, scatter plot showing a weak correlation between CB glomus cells and OSNs. The Pearson correlation coefficient is indicated. *B*, scatter plot showing a weak correlation between CB glomus cells and VSNs. The Pearson correlation coefficient is indicated. *C*, principal component analysis of gene expression patterns for eight single CB glomus cells, two single OSNs, and two single VSNs. The amount of variance explained by principal components 1 and 2 is shown on the *x*- and *y*-axes, respectively.

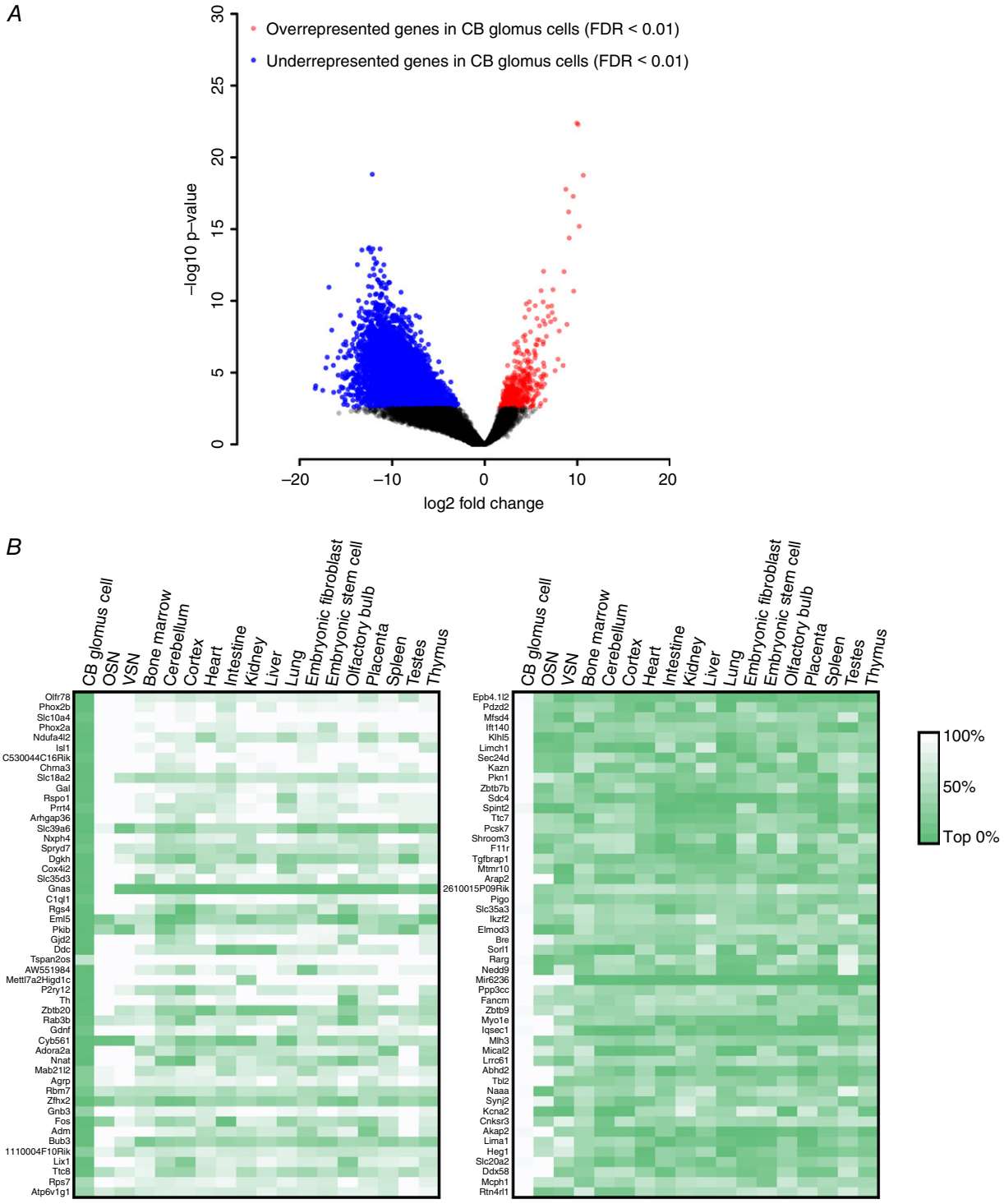

Figure 6. Differential gene expression analysis between single CB glomus cells and non-CB tissues
Differential gene expression analysis was performed using single cell RNA-Seq data from CB glomus cells, OSNs, VSNs as well as public available RNA-Seq data from 15 other mouse tissues. *A*, volcano plot displays $-\log_{10}$ (*P* value) as a function of $\log_2$ (fold change) between CB glomus cells and non-CB tissues, with coloured dots indicating significantly differentially expressed genes (FDR < 0.01). The significantly over-represented genes in CB glomus cells are indicated in red, whereas the significantly under-represented genes in CB glomus cells are indicated in blue. *B*, heat maps showing the expression patterns of the significantly differentially expressed CB glomus cell genes, with the top 50 over-represented genes shown on the left and top 50 under-represented genes shown on the right. Mean expression levels were calculated and their relative rankings in each tissue were shown, with the least abundant gene and other non-detected genes ranked as 100%.

Table 3. Highly expressed G proteins in CB glomus cells

Rank	Gene symbol	Gene name	Average expression (RPM)
1	Gnas	GNAS (guanine nucleotide binding protein, α stimulating) complex locus	18,169
25	Gnb2l1	Guanine nucleotide binding protein (G protein), β polypeptide 2 like 1	1710
50	Gnb1	Guanine nucleotide binding protein (G protein), β-1	1159
86	Gnb2	Guanine nucleotide binding protein (G protein), β-2	853
250	Gnao1	Guanine nucleotide binding protein, α O	500
252	Gng2	Guanine nucleotide binding protein (G protein), γ-2	498
271	Gna11	Guanine nucleotide binding protein, α 11	478
276	Gng3	Guanine nucleotide binding protein (G protein), γ-3	475
386	Gnai2	Guanine nucleotide binding protein (G protein), α inhibiting 2	408
401	Gnai3	Guanine nucleotide binding protein (G protein), α inhibiting 3	396
412	Gnaq	Guanine nucleotide binding protein, α q	389
427	Gng10	Guanine nucleotide binding protein (G protein), γ-10	383
517	Gng12	Guanine nucleotide binding protein (G protein), γ-12	341
966	Gnal	Guanine nucleotide binding protein, α stimulating, olfactory type	237

For Tables 3, 4, 5, 6 and 8, only genes expressed in the top 10% are listed.

Table 4. Highly expressed GPCRs in CB glomus cells

Rank	Gene symbol	Gene name	Average expression (RPM)
13	Olfr78	Olfactory receptor 78	2078
127	Adora2a	Adenosine receptor A2a	689
135	P2ry12	P2Y purinoceptor 12	668
293	Cnr1	Cannabinoid receptor 1	462
312	Adcyap1r1	Pituitary adenylate cyclase-activating polypeptide type I receptor	445
337	Lphn1	Latrophilin-1 precursor	430
849	Lgr5	Leucine-rich repeat-containing G-protein coupled receptor 5 precursor	257

the most abundantly expressed ion channel found was the two-pore domain potassium channel TASK1 (Kcnk3). Another channel of the same family, TREK1 (Kcnk2), was also detected, albeit of lower abundance, consistent with a previous study (Yamamoto & Taniguchi, 2006). Interestingly, other potassium channels detected are mostly voltage-gated potassium channels and calcium-activated potassium channels, both of which have been suggested as additional regulators in CB chemotransduction (Wyatt & Peers, 1995; Sanchez *et al.* 2002). In particular, in the present study, we show that a large number of transcripts encode the inwardly-rectifying hERG channel (Kcnh2). Meanwhile, other types of voltage-gated potassium channels detected include the A-type potassium channels (Kcnc4, Kcnd2) and the delayed rectifier channels (Kcnq5, Kcnq2, Kcnb1, Kcnc1). The presence of large conductance calcium-activated potassium channel Maxi-K is supported by the expression of both its α and β subunits (Kcnma1, Kcnmb2). There is also evidence to suggest the contributions of voltage-gated sodium channels in oxygen sensing by CB glomus cells in rats (Caceres *et al.* 2007). Consistently, we have demonstrated sequencing reads mapping to voltage-gated sodium channel subunits Scn8a, Scn3a, Scn3b and Scn9a in mouse glomus cells.

As expected, several genes encoding the voltage-gated calcium channel subunits were also expressed at high levels, consistent with the notion that calcium influx follows the membrane depolarization step (Buckler & Vaughan-Jones, 1994). Although the high voltage-gated L-type and N-type calcium channels appeared to be most prevalent, we also observed expression of intermediate voltage-gated R-type and low voltage-gated T-type calcium channels, which is consistent with a recent demonstration of the functional involvement of T-type channels in the mouse CB (Makarenko *et al.* 2015). Furthermore, several transient receptor potential channels that may act as additional source of calcium influx were detected. Specifically, Trpm7, Trpc3 and Trpc5 from the TRPM and TRPC subfamilies were expressed.

We also found multiple ligand-gated ion channels in CB glomus cells. These include a highly expressed AMPA-type glutamate receptor (Gria2). Among the less abundant glutamate receptors genes was an NMDA receptor family member Grin1, which was previously reported in rat CB glomus cells (Liu *et al.* 2009). Our data also corroborate

Table 5. Highly expressed GPCR signalling genes in CB glomus cells

Rank	Gene symbol	Gene name	Average expression (RPM)
cAMP-mediated GPCR signalling			
1	Gnas	GNAS (guanine nucleotide binding protein, α stimulating) complex locus	18,169
8	Pkib	cAMP-dependent protein kinase inhibitor β	2371
13	Olfr78	Olfactory receptor 78	2078
70	Prkar1a	cAMP-dependent protein kinase type I-α regulatory subunit	948
127	Adora2a	Adenosine receptor A2a	689
135	P2ry12	P2Y purinoceptor 12	668
163	Prkacb	cAMP-dependent protein kinase catalytic subunit β	601
170	Adcy1	Adenylate cyclase type 1	593
250	Gnao1	Guanine nucleotide binding protein, α O	500
266	Pde1b	Phosphodiesterase 1B, Ca^{2+}-calmodulin-dependent	483
293	Cnr1	Cannabinoid receptor 1	462
312	Adcyap1r1	Pituitary adenylate cyclase-activating polypeptide type I receptor	445
366	Prkaca	Protein kinase, cAMP-dependent, catalytic, α	416
386	Gnai2	Guanine nucleotide binding protein (G protein), α inhibiting 2	408
396	Adrbk2	β-adrenergic receptor kinase 2	401
401	Gnai3	Guanine nucleotide binding protein (G protein), α inhibiting 3	396
663	Akap9	A-kinase anchor protein 9	299
812	Akap11	A kinase (PRKA) anchor protein 11	263
867	Prkar2a	cAMP-dependent protein kinase type II-α regulatory subunit	254
966	Gnal	Guanine nucleotide binding protein, α stimulating, olfactory type	237
1042	Akap8	A kinase (PRKA) anchor protein 8	226
1049	Npy	Pro-neuropeptide Y precursor	225
PKC-mediated GPCR signalling			
14	Dgkk	Diacylglycerol kinase kappa	2048
29	Dgkh	Diacylglycerol kinase eta	1456
126	Prkce	Protein kinase C epsilon type	691
239	Dgkg	Diacylglycerol kinase γ	513
271	Gna11	Guanine nucleotide binding protein, α-11	478
411	Cds2	Phosphatidate cytidylyltransferase 2	390
412	Gnaq	Guanine nucleotide binding protein, α q polypeptide	389
421	Marcks	Myristoylated alanine-rich C-kinase substrate	384
797	Prkca	Protein kinase C α type	266
804	Cdipt	CDP-diacylglycerol–inositol 3-phosphatidyltransferase	265
Regulation of GPCR signalling			
3	Rgs4	Regulator of G-protein signalling 4	7141
37	Rgs5	Regulator of G-protein signalling 5	1337
93	Cd81	CD81 antigen	796
102	Wdr26	WD repeat-containing protein 26	768
149	Gprasp1	G-protein coupled receptor-associated sorting protein 1	637
409	Ric8b	Synembryn-B	391
460	Gde1	Glycerophosphodiester phosphodiesterase 1	369
578	Gprasp2	G-protein coupled receptor-associated sorting protein 2	322
595	Ric8	Synembryn-A	315
646	Arhgef28	Rho guanine nucleotide exchange factor 28	304

the previous suggestion that nicotinic ACh receptors contribute to glomus cell excitation (Wyatt & Peers, 1993) because several subunits of this receptor were detected. Inhibitory receptors subunits (Glrb, Gabrb3) were discovered as well, which belong to the glycine receptor and $GABA_A$ receptor, respectively. Gabrb3 is also one of the less abundant genes whose expression in CB glomus cells has been previously reported in the literature (Igarashi *et al.* 2009).

Taken together, our single cell RNA-Seq identified a CB glomus cell ion channel profile that supports the current understanding of CB membrane conductance.

Furthermore, we identified ion channel transcripts in CB glomus cells that may serve as additional players in regulating membrane potential.

Atypical mitochondrial ETC subunits are among the highly expressed HIF pathway genes in CB glomus cells

In our CB glomus cell RNA-Seq, we found Epas1 (also known as hypoxia-inducible factor 2α, Hif2α) to be the second most abundant transcript. This is corroborated by a strong Epas1 mRNA *in situ* hybridization signal (Fig. 4*C*), as well as previous studies reporting the constitutive expression of Hif2α protein in mouse CB glomus cells (Tian *et al.* 1998; Peng *et al.* 2011). Furthermore, the sequencing result also indicated the presence of other HIF pathway components, such as the hypoxia-inducible factor 1a (Hif1α), the HIFα heterodimer partner aryl hydrocarbon receptor nuclear translocator 2 (Arnt2) and the hypoxia-inducible factor prolyl hydroxylase 2 (PHD2, also known as Egln1). Both HIF1α and HIF2α are transcription factors stabilized under long-term hypoxia to help initiate transcriptions of hypoxia responsive genes. This relatively slow response dynamic of HIFα to hypoxia does not appear to be an ideal feature of acute oxygen sensing. Nonetheless, heterozygous Hif1α and Hif2α deficient mice, respectively, display an altered hypoxic response to chronic and acute hypoxia (Kline *et al.* 2002; Peng *et al.* 2006; Peng *et al.* 2011). HIFs may prove essential as a result of transcribing other genes relevant to CB

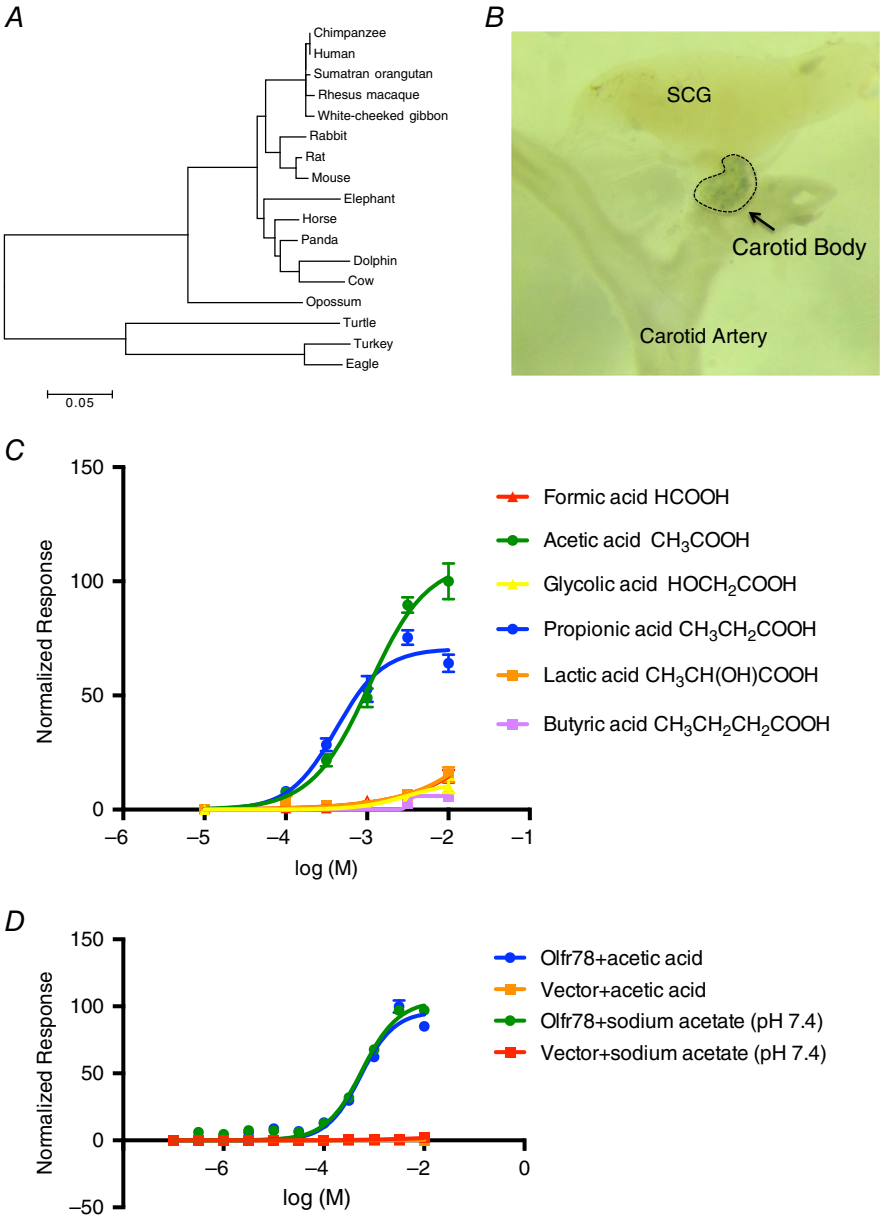

Figure 7. Olfr78 is a conserved olfactory receptor activated by acetate
A, unrooted phylogenetic tree of Olfr78 family orthologs based on similarity of amino acid properties. *B*, lacZ staining of a carotid artery bifurcation from a heterozygous Olfr78^{tm1Mom}/MomJ mouse. Blue precipitation marks the lacZ positive cells. SCG, superior cervical ganglion. *C*, dose–response curves of Olfr78 against SFCA. The *x*-axis represents molar concentration in log scale. *D*, dose–response curves of Olfr78 against acetic acid and sodium acetate (pH 7.4). The *x*-axis represents molar concentration in log scale.

Table 6. Highly expressed ion channels in CB glomus cells

Rank	Gene symbol	Alias	Gene name	Average expression (RPM)
41	Kcnk3	TASK1	Potassium channel subfamily K member 3	1268
61	Scnn1b	ENaC	Sodium channel, nonvoltage-gated 1β	1041
116	Gria2	GluA2	Glutamate receptor 2	711
130	Chrna3	nAChRA3	Neuronal ACh receptor subunit α-3	684
279	Clcn4-2	CLC4	Chloride channel 4-2	473
507	Scn8a	Nav1.6	Sodium channel, voltage-gated, type VIII, α	343
516	Glrb	Glyrb	Glycine receptor subunit β	342
565	Scn3b	Nav1.3	Sodium channel, voltage-gated, type III, β	327
601	Cacna2d1		Voltage-dependent calcium channel subunit α-2/delta-1	314
620	Cacna1b	Cav2.2	Voltage-dependent N-type calcium channel subunit α-1B	310
732	Trpm7		Transient receptor potential cation channel subfamily M member 7	280
799	Scn3a	Nav1.3	Sodium channel, voltage-gated, type III, α	266
997	Kcnc4	Kv3.4	Potassium voltage-gated channel subfamily C member 4	232
1074	Ano6		Anoctamin-6	222

function. Consistent with this, several HIF target genes were also highly expressed in our RNA-Seq data (Table 8), including genes promoting cell growth (Tgfa, Mcl1) and glycolysis (Slc2a3, Ldha, Aldoa). These genes are consistent with the ability of the CB to self-proliferate and sense low glucose (Pardal & Lopez-Barneo, 2002; Pardal *et al.* 2007; Platero-Luengo *et al.* 2014). Unexpectedly, two hypoxia-inducible mitochondrial ETC subunits, Ndufa4l2 and Cox4i2, were among the most highly expressed genes. Their abundance in the CB glomus cells does not require hypoxia induction because constitutive expression was observed under normoxic conditions (Fig. 4*C* and *F*). Based on our meta-analysis of previous studies, although Cox4i2 was moderately expressed in the top 53–63% of whole CB genes, Ndufa4l2 did show relatively high expression in mice CB (Balbir *et al.* 2007; Chang *et al.* 2015). Ndufa4l2 is highly ranked (top 0.28%) in the C57BL6/J whole CB RNA-Seq data (Chang *et al.* 2015). Interestingly, Ndufa4l2 occupied a higher ranking in the high hypoxia responder DBA/2J strain (top 8.47%) than the low hypoxia responder A/J strain (top17.02%). Notably, these two genes were also ranked highly among the list of differentially expressed genes in CB glomus cells, which may imply specialized functions in the CB (Fig. 6*B*). In line with this, the CB mitochondria have demonstrated unusual characteristics, which, along with other evidence, led to the theory that the CB is equipped with specialized mitochondria for sensing moderate hypoxia (Donnelly & Carroll, 2005). Such unique features may require mitochondria that are constituted with alternative molecules. Although it has been demonstrated that Ndufa4l2 and Cox4i2 are crucial for preventing excess reactive oxygen species (ROS) production under hypoxic conditions in other cell types (Fukuda *et al.* 2007; Tello *et al.* 2011), further studies are required to explore their functional significance in the CB, which may lead to novel mechanistic insights.

Overall, the CB glomus cells constitutively overexpress HIFs and certain HIF transcriptional targets that are normally part of the counteractive mechanism against the negative impacts of sustained hypoxia. Specifically, the CB glomus cells transcriptionally upregulate atypical mitochondrial ETC components, emphasizing the previous notion that unique mitochondria are possibly present in the CB and may be responsible for oxygen sensing.

Discussion

A major roadblock to a better understanding of CB function is our scarce knowledge of the glomus cells at the molecular level, which greatly prohibits functional interpretations. There are several reasons that might explain this gap in knowledge, with the small size of the tissue being the most obvious. This problem has been partially circumvented by performing transcriptome profiling experiments using pooled mouse or human CB (Ganfornina *et al.* 2005; Balbir *et al.* 2007; Fagerlund *et al.* 2010; Mkrtchian *et al.* 2012; Chang *et al.* 2015). These studies highlighted species differences and confirmed the expression of many genes relevant to CB function.

In the present study, we explored the possibility of answering this question from a single cell perspective. Using this approach, we obtained the gene expression profile of mouse CB glomus cells. This eliminated the contamination and dilution effects caused by other cell types, and allowed us to uncover gene expression specific to the actual oxygen sensing cells, complementing previous whole-tissue based analyses. In particular, we observed many GPCR signalling pathway components, ion channels and HIF targets, many of which had not been previously

Table 7. Several families of ion channels previously reported in CB were detected by the single glomus cell RNA-Seq

Channel	Family	Subfamily	Gene	Alias	RPM	Gene name	Reference
K^+	Two-pore domain	TASK	Kcnk3	TASK1	1268	Potassium channel subfamily K member 3	Buckler *et al*. (2000)
		TREK	Kcnk2	TREK1	43	Potassium channel subfamily K member 2	Yamamoto & Taniguchi, (2006)
	Voltage-gated	Inward-rectifying	Kcnh2	hERG	182	Potassium voltage-gated channel subfamily H member 2	Overholt *et al*. (2000)
		A-type	Kcnc4	Kv3.4	232	Potassium voltage-gated channel subfamily C member 4	Kaab *et al*. (2005)
		A-type	Kcnd2	Kv4.2	84	Potassium voltage-gated channel subfamily D member 2	Mkrtchian *et al*. (2012)
		Delayed rectifier	Kcnq5	Kv7.5	169	Potassium voltage-gated channel subfamily KQT member 5	Buniel *et al*. (2008)
		Delayed rectifier	Kcnq2	Kv7.2	150	Potassium voltage-gated channel subfamily KQT member 2	Buniel *et al*. (2008)
		Delayed rectifier	Kcnb1	Kv2.1	107	Potassium voltage-gated channel subfamily B member 1	Mkrtchian *et al*. (2012)
		Delayed rectifier	Kcnc1	Kv3.1	107	Potassium voltage-gated channel subfamily C member 1	Pérez-García *et al*. (2004)
	Calcium-activated	Large conductance	Kcnma1	BK, Maxi-K	51	Calcium-activated potassium channel subunit α-1	Peers, (1990)
		Large conductance	Kcnmb2	BK, Maxi-K	85	Calcium-activated potassium channel subunit β-2	Balbir *et al*. (2007)
Na^+	Voltage-gated	Type VIII	Scn8a	Nav1.6	343	Sodium channel, voltage-gated, type VIII, α	Caceres *et al*. (2007)
		Type III	Scn3a	Nav1.3	266	Sodium channel, voltage-gated, type III, α	Caceres *et al*. (2007)
		Type III	Scn3b	Nav1.3	327	Sodium channel, voltage-gated, type III, β	Caceres *et al*. (2007)
		Type IX	Scn9a	Nav1.7	10	Sodium channel, voltage-gated, type IX, α	Caceres *et al*. (2007)
Ca^{2+}	Voltage-gated	α-1, L type	Cacna1d	Cav1.3	184	Voltage-gated L-type calcium channel subunit α-1D	Fieber & McCleskey, (1993)
		α-1, L type	Cacna1c	Cav1.2	131	Voltage-gated L-type calcium channel subunit α-1C	Fieber & McCleskey, (1993)

(Continued)

Table 7. Continued

Channel	Family	Subfamily	Gene	Alias	RPM	Gene name	Reference
		α-1, N Type	Cacna1b	Cav2.2	310	Voltage-gated N-type calcium channel subunit α-1B	Balbir *et al*. (2007)
		α-1, T type	Cacna1i	Cav3.3	48	Voltage-gated T-type calcium channel subunit α-1I	Makarenko *et al*. (2015)
		α-1, T type	Cacna1h	Cav3.2	38	Voltage-gated T-type calcium channel subunit α-1H	Makarenko *et al*. (2015)
		α-1, R Type	Cacna1e	Cav2.3	12	Voltage-gated R-type calcium channel subunit α-1E	Overholt & Prabhakar, (1997)
		α-2/delta	Cacna2d1		314	Voltage-gated calcium channel subunit α-2/delta-1	Buckler & Vaughan-Jones, (1994)
		α-2/delta	Cacna2d3		85	Voltage-gated calcium channel subunit α-2/delta-3	Balbir *et al*. (2007)
		α-2/delta	Cacna2d2		26	Voltage-gated calcium channel subunit α-2/delta-2	Buckler & Vaughan-Jones, (1994)
		β	Cacnb3		148	Voltage-gated L-type calcium channel subunit β-3	Buckler & Vaughan-Jones, (1994)
		γ	Cacng2		52	Voltage-gated calcium channel γ-2 subunit	Buckler & Vaughan-Jones, (1994)
		γ	Cacng4		18	Voltage-gated calcium channel γ-4 subunit	Buckler & Vaughan-Jones, (1994)
TRP		TRPC	Trpc3		47	Short transient receptor potential channel 3	Buniel *et al*. (2003)
		TRPC	Trpc5		22	Short transient receptor potential channel 5	Buniel *et al*. (2003)
Ligand-gated	Glutamate	NMDA	Grin1	GluN1	110	Glutamate receptor, ionotropic, *N*-methyl-D-aspartate 1	Yuzhen Liu *et al*. (2009)
	ACh	Nicotinic	Chrna3	nAChRA3	684	Neuronal ACh receptor subunit α-3	Wyatt & Peers, (1993)
		Nicotinic	Chrna5	nAChRA5	2	Neuronal ACh receptor subunit α-5	Wyatt & Peers, (1993)
		Nicotinic	Chrnb2	nAChRB2	118	Neuronal ACh receptor subunit β-2	Wyatt & Peers, (1993)
		Nicotinic	Chrnb4	nAChRB4	97	Neuronal ACh receptor subunit β-4	Wyatt & Peers, (1993)
	GABA	A	Gabrb3	GABAA	188	γ-aminobutyric acid receptor subunit β-3	Igarashi *et al*. (2009)

Table 8. Highly expressed HIFs and HIF responsive targets in CB glomus cells

Rank	Gene symbol	Gene name	Average expression (RPM)
2	Epas1 (Hif2a)	Endothelial PAS domain-containing protein 1	8096
3	Rgs4	Regulator of G-protein signalling 4	7141
4	Ndufa4l2	NADH dehydrogenase [ubiquinone] 1α subcomplex subunit 4-like 2	5456
37	Rgs5	Regulator of G-protein signalling 5	1337
92	Cox4i2	Cytochrome *c* oxidase subunit IV isoform 2	806
193	Slc2a3	Solute carrier family 2 (facilitated glucose transporter), member 3	566
195	Tgfa	Transforming growth factor α	565
197	Adm	ADM precursor	563
257	Ldha	Lactate dehydrogenase A	491
390	Ctsd	Cathepsin D	404
398	Mcl1	Myeloid cell leukaemia sequence 1	401
413	Vim	Vimentin	388
522	Sod2	Superoxide dismutase 2, mitochondrial	340
561	Aldoa	Fructose-bisphosphate aldolase A	328
635	Ak3	Adenylate kinase 3	306
850	Zeb1	Zinc finger E-box-binding homeobox 1	256
886	L1cam	Neural cell adhesion molecule L1 precursor	251

described in CB glomus cells. Furthermore, we showed that the olfactory receptor Olfr78 was the most abundant GPCR expressed in CB glomus cells and responded to SCFAs such as acetate *in vitro*. We also identified two atypical mitochondrial ETC subunits specifically expressed in CB glomus cells.

Does our single cell RNA-Seq data mimic the *in vivo* transcriptome status? We first sequenced two individual OSNs from the olfactory system. The available literature and transcriptome data of bulk OSNs permit comparisons with our single OSNs data, which suggest substantial similarity, particularly for the more abundant genes. This approach appears feasible because many of the key signalling genes in OSNs were identified. In the case of CB glomus cell, we also observed similar correlation between single glomus cells and whole CB tissue. We further addressed our question by performing *in situ* hybridization and immunohistochemistry for genes and gene products identified from the single cell RNA-Seq, most of which specifically stained the CB glomus cells. *In situ* hybridization is more informative than validation through qRT-PCR, in the sense that it gives information on the origin of the transcript. There were some cases where we saw little to no hybridization signal, possibly as a result of inefficient RNA probe binding or stochastic transcription in the cell that we had sequenced. Another explanation is a result of immediate early response to stimuli during cell preparation, as seen with immediate early genes Fos and Egr1. Fos and Egr1 probes have shown strong hybridization signal in hypoxia-stimulated CB but not in unstimulated CB. Their mRNA occurrences in the single cell RNA-Seq are probably induced by hypoxia or stress associated with the dissociation of single cells. However, we saw a high degree of consistency between the single cell RNA-Seq and *in situ* hybridizations. Collectively, our data suggest that the single cell RNA-Seq approach is a powerful screening tool for uncovering abundant transcripts in specific cell types of interest, including CB glomus cells, although caution is warranted for less abundant genes because a no sequence read in our transcriptome data does not necessarily mean no expression.

Our approach also exhibits some potential issues that warrant careful scrutiny of the results. Similar to most single cell RNA-Seq, there is more variability compared to traditional whole tissue RNA-Seq partly as a result of cell-to-cell heterogeneity among apparently homogeneous cells (Cai *et al.* 2006; Wang & Bodovitz, 2010; Tang *et al.* 2011; Shalek *et al.* 2013). Furthermore, more abundant transcripts show stronger correlation between replicates, whereas more discrepancy occurred for genes with low read counts, leading to increased variability and a lower detection rate among weakly expressed genes. Technical noises resulting from small starting RNA material and cDNA amplification biases can account for such variability. It has been demonstrated that RNA-Seq sensitivity decreases substantially when the starting amount of RNAs declines to the picogram level (Ramskold *et al.* 2012). Additionally, because of the multiple rounds of cDNA amplification, it is inevitable that amplification efficiency differences and PCR byproducts deter faithful representation of the original expression profile. However, these effects have a lower probability of hindering the amplification of more abundant transcripts. Also, considering that molecules with crucial functions are often associated with abundant transcripts, as has been demonstrated in the OSNs, the preferential influence

of technical limitations on the weakly expressed genes becomes less concerning.

The expression profile provided by our single glomus cell RNA-Seq suggests a unique transcriptome signature. Previous studies comparing human CB transcriptome with those of other tissues have found little similarity (Mkrtchian *et al.* 2012). In line with this, our principal component analysis and correlation coefficients also showed clear differences between CB glomus cells and OSNs/VSNs, supporting a unique transcriptome profile. To highlight the differentially expressed genes, we compared the glomus cells with 17 other tissues and cell types. These differentially expressed CB glomus cell genes may possibly contribute to its distinguishing features. Importantly, the differentially expressed genes contain those that have not been previously described in CB glomus cells, such as Ndufa4l2 and Cox4i2.

Our CB glomus cell data emphasize a long-held notion that G protein-mediated signalling is heavily involved in CB chemotransduction (Cachero *et al.* 1995; Prabhakar *et al.* 1995; Cachero *et al.* 1996). Although G proteins have been suggested to be present in CB tissue, direct evidence is still limited, especially regarding the types of G proteins present. In the present study, we describe a list of heterotrimeric G protein complex subunits expressed at high levels in CB glomus cells. Although members of all four major G protein families were present in CB glomus cells, $G_{\alpha s,}$ which activates adenyl cyclase, was most appreciably expressed. Aside from $G_{\alpha s}$ and $G_{\alpha olf}$, we also detected many transcripts encoding $G_{\alpha i/o}$ that inhibit adenyl cyclase activity, enabling the negative regulation of cAMP. These, combined with our analysis of the highly ranked GPCR signalling molecules, suggest a prominent role of cAMP-mediated GPCR signalling in modulating CB chemotransduction. Although some controversies exist, cAMP has been described to increase under a hypoxic stimulus and to contribute to chemosensory discharge in CB (Wang *et al.* 1989; Pérez-García *et al.* 1990; Delpiano & Acker, 1991; Pérez-García *et al.* 1991). An increased cAMP level is associated with the inhibition of hypoxia-sensitive potassium channels and enhanced neurotransmitter release from CB glomus cells (Lopez-Lopez *et al.* 1993; Rocher *et al.* 2009). Meanwhile, an alternative signal transduction acting through the PKC-mediated pathway also appears to co-exist, potentially contributing to an additional source of calcium release that facilitates CB activation. Interestingly, PKC has also been implicated in potentiating CB glomus cells response through diverse targets (Peers & Carpenter, 1998; Faff *et al.* 1999; Summers *et al.* 2000; Roy *et al.* 2013). Overall, our data indicate that CB glomus cells are equipped with vast GPCR signal transduction components. More research is clearly needed to differentiate the role of individual signalling pathways and molecules with regard to different CB stimuli and how distinct chemotransduction pathways are integrated in this polymodal sensory tissue.

The various neurotransmitters and peptides secreted by CB glomus cells and nearby tissues have shown ability to exert autocrine or paracrine effects on CB glomus cells. A significant portion of these effects is mediated through activation of corresponding GPCRs, with those that increase cAMP levels exerting excitatory effects, and vice versa (Cachero *et al.* 1996; Nurse, 2005; Nunes *et al.* 2014). This phenomenon is in agreement with the high levels of such receptors detected in the present study. Among the highly expressed GPCRs identified, the adenosine and ATP receptors (Adora2a, P2ry12) have long been known to modulate CB response to hypoxia (Monteiro & Ribeiro, 1987; Conde & Monteiro, 2004; Xu *et al.* 2005; Conde *et al.* 2006). Interestingly, our data also corroborate recent findings of several GPCRs in CB glomus cells with implications in respiratory control, highlighting the importance of GPCR signalling in CB function. The most persuasive evidence comes from recent work showing that Olfr78 mutant mice fail to hyperventilate under hypoxia as a result of lactate insensitive CB (Chang *et al.* 2015). In addition, the highly abundant cAMP-inhibiting cannabinoid receptor 1 (Cnr1) was also detected in rat CB glomus cells, where a possible link between perinatal exposure to marijuana and sudden infant death syndrome was suggested (McLemore *et al.* 2004). Another particularly intriguing receptor is the PACAP receptor (Adcyap1r1) that couples to $G_{\alpha s}$. This receptor binds to PACAP, a secretory peptide important for respiratory chemoresponses (Cummings *et al.* 2004; Arata *et al.* 2013). PACAP and its receptor have also been shown to be present in rat CB (Lam *et al.* 2012). Interestingly, PACAP alone is sufficient to demonstrate stimulatory effects on CB glomus cells that could be attenuated upon PKA inhibition, further suggesting the importance of cAMP in CB chemosensory transduction (Lam *et al.* 2012). Although an increase in cAMP is associated with increased glomus cell activation, the CB can also take advantage of the inhibitory autocrine regulation via $G_{\alpha i}$-coupled receptors (e.g. dopamine receptor; Drd2), to maintain a sustained slow-adapting hypoxia response through a push and pull mechanism (Carroll *et al.* 2005).

We found olfactory receptor Olfr78 to be the most abundantly expressed GPCR in CB glomus cells as shown in the single cell RNA-Seq data, Olfr78 *in situ* hybridization and lacZ staining of Olfr78 transgenic mouse CB. Published whole CB transcriptome data corroborate this finding in C57BL6/J, DBA/2J and A/J strains of mice (Balbir *et al.* 2007; Chang *et al.* 2015). Furthermore, Olfr78 was found to be upregulated in mice CB *vs.* brain, although it was not included when human CB was compared with the brain (Mkrtchian *et al.* 2012). The mRNA abundance of OR51E2 (human orthologue of Olfr78) may be undermined in the whole tissue setting, especially considering

the fact that these CB derived from older adults (aged 48–68 years), because there may be more connective tissues and fats. Although we were unable to attest to the expression of Olfr78 in human CB as a result of lack of open resources, we confirmed its presence in rats using the available public microarray data of cultured rat CB cells (GEO ID: GSE67429).

Our analysis also indicates that Olfr78 was the most differentially expressed gene over-represented in CB glomus cells, indicative of specialized function. Unlike most other olfactory receptors, Olfr78 is well conserved and translocates to the cell surface without additional receptor transport proteins (Pluznick *et al.* 2013). Olfr78 was previously detected in several small non-olfactory tissues, including specialized renal cells, where it demonstrated functional significance outside of the olfaction system (Conzelmann *et al.* 2000; Weber *et al.* 2002; Neuhaus *et al.* 2009; Pluznick *et al.* 2013). Our hypothesis of Olfr78 contributing to CB chemosensory function is further supported by a recent study also demonstrating Olfr78 enrichment in the mouse CB, where it indirectly senses hypoxia via lactate (Chang *et al.* 2015). Although we also observed weak activation of Olfr78 by lactic acid, its response is considerably smaller compared to other SCFA ligands, acetic acid and propionic acid. SCFA, derived from the fermentation of complex polysaccharides by gut microbes, are normal constituents of arterial blood with significant implications in many physiological activities (Tremaroli & Backhed, 2012). Being the major SCFA entering circulation, the arterial acetate concentrations fall between 0.1 and 0.5 mM in non-herbivores and are within the responsive range of Olfr78 (Ballard, 1972), making it a good candidate for monitoring blood acetate levels. Of particular interest, the blood acetate level was shown to increase in newborn rats given a hypoxic challenge (Knowles *et al.* 1974). Although there are currently no definitive links between the acetate level and CB-mediated breathing control at the whole animal level, acetate applied to rabbit CB glomus cells at pH 7.4 has led to increase in intracellular calcium (Sato, 1994). A recent study by Chang *et al.* (2015) also directly showed that Olfr78 is responsible for CB sensory activity to lactate and acetate, and mice lacking this receptor do not hyperventilate under hypoxia. Although lower than those of lactate, blood acetate levels may elicit robust Olfr78 activation. Hence, it is intriguing to speculate that acetate may be capable of modulating CB chemosensory function through Olfr78 in a similar fashion to other metabotropic receptor ligands that act on CB.

Although little is known about the identity of the actual oxygen sensor in glomus cells, it is generally agreed that oxygen-sensitive potassium channels are important downstream effectors. However, some degree of variation has been observed as a result of strain, species and experimental differences. Our single cell RNA-Seq data described which ion channels are expressed in mouse CB glomus cells. In multiple species, TASK channels have been demonstrated to be the predominant oxygen-sensitive channels (Buckler *et al.* 2000; Kobayashi & Yamamoto, 2010). In line with this, the most abundant ion channel detected in our single CB glomus cells was TASK1 (Kcnk3). However, TASK3 (Kcnk9) was not detected. This is similar to human CB microarray data showing the expression of TASK1 but not TASK3 (Mkrtchian *et al.* 2012). Although studies using mutant mice have shown that both TASK1 and TASK3 contribute to background potassium currents, the latter has a smaller conductance and is less sensitive to hypoxia and mitochondrial inhibitors (Turner & Buckler, 2013). If expressed at a low level, it is possible for our single cell RNA-Seq method to underestimate its presence. In addition to background potassium channels, the mouse CB glomus cells also expressed several members from different voltage-gated potassium channels and calcium-activated potassium channels families. For example, the presence of Kcnh2 transcripts supports the characterization of hERG-like currents in regulating the resting membrane potential of CB glomus cells (Overholt *et al.* 2000).

Other than potassium channels, we also detected various other types of ion channels in our sequencing reads, including sodium channels, TRP channels and ligand-gated ion channels. This information can be of great value for future studies because these ion channels may also regulate the electrical signalling in CB glomus cells. Intriguingly, the detection of TRP channels in CB glomus cells may prove to be of functional importance through their diverse sensitivity to a wide array of stimuli. Both a TRPM channel (Trpm7) and a TRPC channel (Trpc3) were detected in our experiment, consistent with a previous report of multiple TRPC channels in rat CB glomus cells (Buniel *et al.* 2003). The TRPM7 channel has been implicated in meditating anoxia sensing in the brain, whereas the TRPC6 channel is suggested to be essential to hypoxic pulmonary vasoconstriction in the pulmonary smooth muscle cells (Takahashi *et al.* 2012). Our glomus cell transcriptome profile also indicates the presence of both excitatory and inhibitory ligand-gated ion channels. Specifically, the data highlight the presence of glutamate, ACh and glycine receptors in CB glomus cells, whose roles in CB transduction remain to be explored.

Mitochondria have long been proposed as the oxygen sensor in CB glomus cells. Not only do mitochondria consume most of the cellular oxygen, but also their inhibitors activate CB, as does hypoxia. However, the mitochondria theory succumbs to major criticism because of the ubiquitous presence of mitochondria and their high oxygen affinity. Although evidence has emerged indicating the presence of specialized mitochondria in CB glomus cells (Mills & Jobsis, 1970, 1972; Duchen & Biscoe, 1992*a*,*b*; Streller *et al.* 2002; Buckler & Turner,

2013), molecular evidence is still lacking. A key finding from our single CB glomus cell RNA-Seq is the abundant and constitutive expression of two atypical mitochondrial ETC subunits, Ndufa4l2 and Cox4i2, which are also among the most differentially expressed genes over-represented in CB glomus cells. Ndufa4l2 and Cox4i2 are both nuclear encoded mitochondrial ETC subunits that are induced by HIF1α after several hours of hypoxic challenge in various cells or tissues. Their significance lies in their ability to keep hypoxia induced ROS production in check (Fukuda *et al.* 2007; Tello *et al.* 2011). Specifically, Ndufa4l2 was shown to limit ROS production by attenuating mitochondrial activity, which also results in decreases in oxygen consumption and mitochondrial membrane potential (Tello *et al.* 2011). Hence, constitutive Ndufa4l2 expression might also attenuate CB glomus cell mitochondria activity, making it more susceptible to additional changes in oxygen tension. The observed high expression levels of glycolysis genes may also reflect weakened mitochondrial oxidative phosphorylation. Ndufa4l2 was previously categorized as a complex I component of mitochondrial ETC because of its sequence similarity to its paralogue, Ndufa4 (Tello *et al.* 2011). In line with this, another mitochondrial complex I component, Ndufs2, was recently characterized as a critical player in CB oxygen sensing and signals hypoxia stimulus through the cellular redox state (Fernandez-Aguera *et al.* 2015). This, combined with our transcriptome results, further iterates the importance of mitochondria in acute oxygen sensing. Of note, recent studies have demonstrated that the Ndufa4l2 paralogue, Ndufa4, belongs to complex IV of the mammalian mitochondrial ETC (Balsa *et al.* 2012; Pitceathly *et al.* 2013). Thus, it is possible that Ndufa4l2 could also be a complex IV component, as it is in the case of Cox4i2. A unique feature of complex IV is its role as the site of oxygen reduction. Therefore, these two proteins may also affect CB glomus cell mitochondrial functions, especially those pertaining to oxygen affinity.

The most perplexing question about the CB is the identity of the oxygen sensor and its immediate components. Previous efforts aiming to understand the nature of these sensors have generated multiple theories on how acute hypoxia is sensed in CB. Our single CB glomus cell RNA-Seq data provide a list of candidate genes that may serve such functions. One of the major theories is the metabolic theory. In support of this theory, we identified two highly expressed atypical mitochondrial ETC subunits in CB glomus cells that may contribute to specialized mitochondria. Metabolic theory also suggests that increased AMP/ATP ratio under hypoxia activates AMP-activated protein kinase (AMPK), which may phosphorylate potassium channels (Wyatt *et al.* 2007). In line with this, we detected transcripts encoding the α, β and γ subunits of AMPK. NADPH oxidase has also been considered to be a potential oxygen sensor as a result of its ability to translate oxygen level into reactive oxygen species. Yet, similar to previous CB transcriptome studies, we could only detect NADPH oxidase 4 (Nox4) in mouse CB glomus cells. Recently, greater emphasis has been given to H_2S, CO and NO as gasotransmitters in the CB oxygen sensing process (Peng *et al.* 2010; Prabhakar & Peers, 2014; Yuan *et al.* 2015). However, we observed few to no reads for the genes responsible for generating these gases (i.e. Cbs, Cth, Hmox2, Nos1, Nos2 and Nos3). Previous mouse CB microarray experiments also failed to detect the H_2S generating enzyme Cth in mice, and Cbs was not detected in the DBA/2J and A/J strains. Possible explanations for this discrepancy could be either strain differences, or the relatively lower sensitivity of the single cell RNA-Seq approach for less abundant genes, resulting in drop out incidences. Lastly, we detected the significant presence of an olfactory receptor Olfr78, which was recently proposed to be a novel CB oxygen sensor (Chang *et al.* 2015).

In conclusion, we have established a method of sequencing single sensory cells isolated from heterogeneous tissues. In the present study, we show that this method could be effectively used to estimate the overall gene expression from a single cell as had been demonstrated with OSNs. Using this approach, we characterized the transcriptome profile of mouse CB glomus cells, generating substantial novel information regarding the types of molecules present in this much-understudied tissue. The CB glomus cell transcriptome is unique compared to other cell types, containing a set of differentially expressed genes. Transcriptome analysis revealed the significant involvement of GPCR signalling in CB glomus cells, especially pertaining to the cAMP-mediated pathway. Overall, our CB transcriptome profile not only demonstrated similarity to the current literature, but also identified many novel CB glomus cell genes with potential functional importance, such as the atypical mitochondrial ETC subunits. The results of the present study will serve as a rich resource for future research investigating the molecular mechanisms of CB glomus cell transduction.

References

Anders S & Huber W (2010). Differential expression analysis for sequence count data. *Genome Biol* **11**, R106.

Arata S, Nakamachi T, Onimaru H, Hashimoto H & Shioda S (2013). Impaired response to hypoxia in the respiratory center is a major cause of neonatal death of the PACAP-knockout mouse. *Eur J Neurosci* **37**, 407–416.

Balbir A, Lee H, Okumura M, Biswal S, Fitzgerald RS & Shirahata M (2007). A search for genes that may confer divergent morphology and function in the carotid body between two strains of mice. *Am J Physiol Lung Cell Mol Physiol* **292**, L704–L715.

Ballard FJ (1972). Supply and utilization of acetate in mammals. *Am J Clin Nutr* **25**, 773–779.

Balsa E, Marco R, Perales-Clemente E, Szklarczyk R, Calvo E, Landazuri MO & Enriquez JA (2012). NDUFA4 is a subunit of complex IV of the mammalian electron transport chain. *Cell Metab* **16**, 378–386.

Bozza T, Vassalli A, Fuss S, Zhang JJ, Weiland B, Pacifico R, Feinstein P & Mombaerts P (2009). Mapping of class I and class II odorant receptors to glomerular domains by two distinct types of olfactory sensory neurons in the mouse. *Neuron* **61**, 220–233.

Buckler KJ (2007). TASK-like potassium channels and oxygen sensing in the carotid body. *Respir Physiol Neurobiol* **157**, 55–64.

Buckler KJ & Turner PJ (2013). Oxygen sensitivity of mitochondrial function in rat arterial chemoreceptor cells. *J Physiol* **591**, 3549–3563.

Buckler KJ & Vaughan-Jones RD (1994). Effects of hypoxia on membrane potential and intracellular calcium in rat neonatal carotid body type I cells. *J Physiol* **476**, 423–428.

Buckler KJ, Williams BA & Honore E (2000). An oxygen-, acid- and anaesthetic-sensitive TASK-like background potassium channel in rat arterial chemoreceptor cells. *J Physiol* **525**, 135–142.

Buniel M, Glazebrook PA, Ramirez-Navarro A & Kunze DL (2008). Distribution of voltage-gated potassium and hyperpolarization-activated channels in sensory afferent fibers in the rat carotid body. *J Comp Neurol* **510**, 367–377.

Buniel MC, Schilling WP & Kunze DL (2003). Distribution of transient receptor potential channels in the rat carotid chemosensory pathway. *J Comp Neurol* **464**, 404–413.

Caceres AI, Obeso A, Gonzalez C & Rocher A (2007). Molecular identification and functional role of voltage-gated sodium channels in rat carotid body chemoreceptor cells. Regulation of expression by chronic hypoxia in vivo. *J Neurochem* **102**, 231–245.

Cachero TG, Rigual R, Rocher A & Gonzalez C (1996). Cholera and pertussis toxins reveal multiple regulation of cAMP levels in the rabbit carotid body. *Eur J Neurosci* **8**, 2320–2327.

Cachero TG, Rocher A, Rigual RJ & Gonzalez C (1995). Effects of fluoride and cholera and pertussis toxins on sensory transduction in the carotid body. *Am J Physiol Cell Physiol* **269**, C1271–C1279.

Cai L, Friedman N & Xie XS (2006). Stochastic protein expression in individual cells at the single molecule level. *Nature* **440**, 358–362.

Carroll JL, Boyle KM, Wasicko MJ & Sterni LM (2005). Dopamine D2 receptor modulation of carotid body type 1 cell intracellular calcium in developing rats. *Am J Physiol Lung Cell Mol Physiol* **288**, L910–L916.

Chandel NS & Schumacker PT (2000). Cellular oxygen sensing by mitochondria: old questions, new insight. *J Appl Physiol (1985)* **88**, 1880–1889.

Chang AJ, Ortega FE, Riegler J, Madison DV & Krasnow MA (2015). Oxygen regulation of breathing through an olfactory receptor activated by lactate. *Nature* **527**, 240–244.

Chen J, He L, Dinger B, Stensaas L & Fidone S (2002). Role of endothelin and endothelin A-type receptor in adaptation of the carotid body to chronic hypoxia. *Am J Physiol Lung Cell Mol Physiol* **282**, L1314–L1323.

Conde SV & Monteiro EC (2004). Hypoxia induces adenosine release from the rat carotid body. *J Neurochem* **89**, 1148–1156.

Conde SV, Obeso A, Vicario I, Rigual R, Rocher A & Gonzalez C (2006). Caffeine inhibition of rat carotid body chemoreceptors is mediated by A2A and A2B adenosine receptors. *J Neurochem* **98**, 616–628.

Conzelmann S, Levai O, Bode B, Eisel U, Raming K, Breer H & Strotmann J (2000). A novel brain receptor is expressed in a distinct population of olfactory sensory neurons. *Eur J Neurosci* **12**, 3926–3934.

Cummings KJ, Pendlebury JD, Sherwood NM & Wilson RJ (2004). Sudden neonatal death in PACAP-deficient mice is associated with reduced respiratory chemoresponse and susceptibility to apnoea. *J Physiol* **555**, 15–26.

Delpiano MA & Acker H (1991). Hypoxia increases the cyclic AMP content of the cat carotid body in vitro. *J Neurochem* **57**, 291–297.

Dempsey JA, Smith CA, Blain GM, Xie A, Gong Y & Teodorescu M (2012). Role of central/peripheral chemoreceptors and their interdependence in the pathophysiology of sleep apnea. *Adv Exp Med Biol* **758**, 343–349.

Donnelly DF & Carroll JL (2005). Mitochondrial function and carotid body transduction. *High Alt Med Biol* **6**, 121–132.

Duchen MR & Biscoe TJ (1992*a*). Mitochondrial function in type I cells isolated from rabbit arterial chemoreceptors. *J Physiol* **450**, 13–31.

Duchen MR & Biscoe TJ (1992*b*). Relative mitochondrial membrane potential and $[Ca^{2+}]_i$ in type I cells isolated from the rabbit carotid body. *J Physiol* **450**, 33–61.

Faff L, Kowalewski C & Pokorski M (1999). Protein kinase C – a potential modifier of carotid body function. *Monaldi Arch Chest Dis* **54**, 172–177.

Fagerlund MJ, Kahlin J, Ebberyd A, Schulte G, Mkrtchian S & Eriksson LI (2010). The human carotid body: expression of oxygen sensing and signaling genes of relevance for anesthesia. *Anesthesiology* **113**, 1270–1279.

Fernandez-Aguera MC, Gao L, Gonzalez-Rodriguez P, Pintado CO, Arias-Mayenco I, Garcia-Flores P, Garcia-Perganeda A, Pascual A, Ortega-Saenz P & Lopez-Barneo J (2015). Oxygen sensing by arterial chemoreceptors depends on mitochondrial complex I signaling. *Cell Metab* **22**, 825–837.

Fieber LA & McCleskey EW (1993). L-type calcium channels in type I cells of the rat carotid body. *J Neurophysiol* **70**, 1378–1384.

Fukuda R, Zhang H, Kim JW, Shimoda L, Dang CV & Semenza GL (2007). HIF-1 regulates cytochrome oxidase subunits to optimize efficiency of respiration in hypoxic cells. *Cell* **129**, 111–122.

Fung ML, Lam SY, Chen Y, Dong X & Leung PS (2001). Functional expression of angiotensin II receptors in type-I cells of the rat carotid body. *Pflügers Arch* **441**, 474–480.

Ganfornina MD, Pérez-García MT, Gutierrez G, Miguel-Velado E, Lopez-Lopez JR, Marin A, Sanchez D & Gonzalez C (2005). Comparative gene expression profile of mouse carotid body and adrenal medulla under physiological hypoxia. *J Physiol* **566**, 491–503.

Gauda EB, Bamford O & Gerfen CR (1996). Developmental expression of tyrosine hydroxylase, D2-dopamine receptor and substance P genes in the carotid body of the rat. *Neuroscience* **75**, 969–977.

Hanchate NK, Kondoh K, Lu Z, Kuang D, Ye X, Qiu X, Pachter L, Trapnell C & Buck LB (2015). Single-cell transcriptomics reveals receptor transformations during olfactory neurogenesis. *Science* **350**, 1251–1255.

Igarashi A, Zadzilka N & Shirahata M (2009). Benzodiazepines and GABA-GABAA receptor system in the cat carotid body. *Adv Exp Med Biol* **648**, 169–175.

Jaitin DA, Kenigsberg E, Keren-Shaul H, Elefant N, Paul F, Zaretsky I, Mildner A, Cohen N, Jung S, Tanay A & Amit I (2014). Massively parallel single-cell RNA-seq for marker-free decomposition of tissues into cell types. *Science* **343**, 776–779.

Kaab S, Miguel-Velado E, Lopez-Lopez JR & Pérez-García MT (2005). Down regulation of Kv3.4 channels by chronic hypoxia increases acute oxygen sensitivity in rabbit carotid body. *J Physiol* **566**, 395–408.

Kemp PJ & Telezhkin V (2014). Oxygen sensing by the carotid body: is it all just rotten eggs? *Antioxid Redox Signal* **20**, 794–804.

Kline DD, Peng YJ, Manalo DJ, Semenza GL & Prabhakar NR (2002). Defective carotid body function and impaired ventilatory responses to chronic hypoxia in mice partially deficient for hypoxia-inducible factor 1 alpha. *Proc Natl Acad Sci USA* **99**, 821–826.

Knowles SE, Jarrett IG, Filsell OH & Ballard FJ (1974). Production and utilization of acetate in mammals. *Biochem J* **142**, 401–411.

Kobayashi N & Yamamoto Y (2010). Hypoxic responses of arterial chemoreceptors in rabbits are primarily mediated by leak K channels. *Adv Exp Med Biol* **669**, 195–199.

Lam SY, Liu Y, Liong EC, Tipoe GL & Fung ML (2012). Upregulation of pituitary adenylate cyclase activating polypeptide and its receptor expression in the rat carotid body in chronic and intermittent hypoxia. *Adv Exp Med Biol* **758**, 301–306.

Liu Y, Ji ES, Xiang S, Tamisier R, Tong J, Huang J & Weiss JW (2009). Exposure to cyclic intermittent hypoxia increases expression of functional NMDA receptors in the rat carotid body. *J Appl Physiol (1985)* **106**, 259–267.

Lopez-Barneo J, Ortega-Saenz P, Pardal R, Pascual A, Piruat JI, Duran R & Gomez-Diaz R (2009). Oxygen sensing in the carotid body. *Ann NY Acad Sci* **1177**, 119–131.

Lopez-Lopez JR, De Luis DA & Gonzalez C (1993). Properties of a transient K^+ current in chemoreceptor cells of rabbit carotid body. *J Physiol* **460**, 15–32.

Magklara A, Yen A, Colquitt BM, Clowney EJ, Allen W, Markenscoff-Papadimitriou E, Evans ZA, Kheradpour P, Mountoufaris G, Carey C, Barnea G, Kellis M & Lomvardas S (2011). An epigenetic signature for monoallelic olfactory receptor expression. *Cell* **145**, 555–570.

Makarenko VV, Peng YJ, Yuan G, Fox AP, Kumar GK, Nanduri J & Prabhakar NR (2015). CaV3.2 T-type Ca(2)(+) channels in H(2)S-mediated hypoxic response of the carotid body. *Am J Physiol Cell Physiol* **308**, C146–C154.

McLemore GL, Cooper RZ, Richardson KA, Mason AV, Marshall C, Northington FJ & Gauda EB (2004). Cannabinoid receptor expression in peripheral arterial chemoreceptors during postnatal development. *J Appl Physiol (1985)* **97**, 1486–1495.

Mills E & Jobsis FF (1970). Simultaneous measurement of cytochrome a3 reduction and chemoreceptor afferent activity in the carotid body. *Nature* **225**, 1147–1149.

Mills E & Jobsis FF (1972). Mitochondrial respiratory chain of carotid body and chemoreceptor response to changes in oxygen tension. *J Neurophysiol* **35**, 405–428.

Mkrtchian S, Kahlin J, Ebberyd A, Gonzalez C, Sanchez D, Balbir A, Kostuk EW, Shirahata M, Fagerlund MJ & Eriksson LI (2012). The human carotid body transcriptome with focus on oxygen sensing and inflammation – a comparative analysis. *J Physiol* **590**, 3807–3819.

Monteiro EC & Ribeiro JA (1987). Ventilatory effects of adenosine mediated by carotid body chemoreceptors in the rat. *Naunyn Schmiedebergs Arch Pharmacol* **335**, 143–148.

Neuhaus EM, Zhang W, Gelis L, Deng Y, Noldus J & Hatt H (2009). Activation of an olfactory receptor inhibits proliferation of prostate cancer cells. *J Biol Chem* **284**, 16218–16225.

Nunes AR, Holmes AP, Conde SV, Gauda EB & Monteiro EC (2014). Revisiting cAMP signaling in the carotid body. *Front Physiol* **5**, 406.

Nurse CA (2005). Neurotransmission and neuromodulation in the chemosensory carotid body. *Auton Neurosci* **120**, 1–9.

Overholt JL, Ficker E, Yang T, Shams H, Bright GR & Prabhakar NR (2000). HERG-like potassium current regulates the resting membrane potential in glomus cells of the rabbit carotid body. *J Neurophysiol* **83**, 1150–1157.

Overholt JL & Prabhakar NR (1997). Ca^{2+} current in rabbit carotid body glomus cells is conducted by multiple types of high-voltage-activated Ca^{2+} channels. *J Neurophysiol* **78**, 2467–2474.

Pardal R & Lopez-Barneo J (2002). Low glucose-sensing cells in the carotid body. *Nat Neurosci* **5**, 197–198.

Pardal R, Ortega-Saenz P, Duran R & Lopez-Barneo J (2007). Glia-like stem cells sustain physiologic neurogenesis in the adult mammalian carotid body. *Cell* **131**, 364–377.

Patel AP, Tirosh I, Trombetta JJ, Shalek AK, Gillespie SM, Wakimoto H, Cahill DP, Nahed BV, Curry WT, Martuza RL, Louis DN, Rozenblatt-Rosen O, Suva ML, Regev A & Bernstein BE (2014). Single-cell RNA-seq highlights intratumoral heterogeneity in primary glioblastoma. *Science* **344**, 1396–1401.

Peers C (1990). Hypoxic suppression of K^+ currents in type I carotid body cells: selective effect on the Ca2(+)-activated K^+ current. *Neurosci Lett* **119**, 253–256.

Peers C & Carpenter E (1998). Inhibition of Ca^{2+}-dependent K^+ channels in rat carotid body type I cells by protein kinase C. *J Physiol* **512**, 743–750.

Peng YJ, Nanduri J, Khan SA, Yuan G, Wang N, Kinsman B, Vaddi DR, Kumar GK, Garcia JA, Semenza GL & Prabhakar NR (2011). Hypoxia-inducible factor 2alpha (HIF-2alpha) heterozygous-null mice exhibit exaggerated carotid body sensitivity to hypoxia, breathing instability, and hypertension. *Proc Natl Acad Sci USA* **108**, 3065–3070.

Peng YJ, Nanduri J, Raghuraman G, Souvannakitti D, Gadalla MM, Kumar GK, Snyder SH & Prabhakar NR (2010). H_2S mediates O_2 sensing in the carotid body. *Proc Natl Acad Sci USA* **107**, 10719–10724.

Peng YJ, Yuan G, Ramakrishnan D, Sharma SD, Bosch-Marce M, Kumar GK, Semenza GL & Prabhakar NR (2006). Heterozygous HIF-1alpha deficiency impairs carotid body-mediated systemic responses and reactive oxygen species generation in mice exposed to intermittent hypoxia. *J Physiol* **577**, 705–716.

Pérez-García MT, Almaraz L & Gonzalez C (1990). Effects of different types of stimulation on cyclic AMP content in the rabbit carotid body: functional significance. *J Neurochem* **55**, 1287–1293.

Pérez-García MT, Almaraz L & Gonzalez C (1991). Cyclic AMP modulates differentially the release of dopamine induced by hypoxia and other stimuli and increases dopamine synthesis in the rabbit carotid body. *J Neurochem* **57**, 1992–2000.

Pérez-García MT, Colinas O, Miguel-Velado E, Moreno-Dominguez A & Lopez-Lopez JR (2004). Characterization of the Kv channels of mouse carotid body chemoreceptor cells and their role in oxygen sensing. *J Physiol* **557**, 457–471.

Pitceathly RD, Rahman S, Wedatilake Y, Polke JM, Cirak S, Foley AR, Sailer A, Hurles ME, Stalker J, Hargreaves I, Woodward CE, Sweeney MG, Muntoni F, Houlden H, Taanman JW, Hanna MG & Consortium UK (2013). NDUFA4 mutations underlie dysfunction of a cytochrome c oxidase subunit linked to human neurological disease. *Cell Rep* **3**, 1795–1805.

Platero-Luengo A, Gonzalez-Granero S, Duran R, Diaz-Castro B, Piruat JI, Garcia-Verdugo JM, Pardal R & Lopez-Barneo J (2014). An O_2-sensitive glomus cell-stem cell synapse induces carotid body growth in chronic hypoxia. *Cell* **156**, 291–303.

Pluznick JL, Protzko RJ, Gevorgyan H, Peterlin Z, Sipos A, Han J, Brunet I, Wan LX, Rey F, Wang T, Firestein SJ, Yanagisawa M, Gordon JI, Eichmann A, Peti-Peterdi J & Caplan MJ (2013). Olfactory receptor responding to gut microbiota-derived signals plays a role in renin secretion and blood pressure regulation. *Proc Natl Acad Sci USA* **110**, 4410–4415.

Prabhakar NR (2013). Sensing hypoxia: physiology, genetics and epigenetics. *J Physiol* **591**, 2245–2257.

Prabhakar NR, Kou YR & Kumar GK (1995). G proteins in carotid body chemoreception. *Biol Signals* **4**, 271–276.

Prabhakar NR & Peers C (2014). Gasotransmitter regulation of ion channels: a key step in O_2 sensing by the carotid body. *Physiology (Bethesda)* **29**, 49–57.

Prabhakhar NR & Joyner MJ (2014). Tasting arterial blood: what do the carotid chemoreceptors sense? *Front Physiol* **5**, 524.

Ramskold D, Luo S, Wang YC, Li R, Deng Q, Faridani OR, Daniels GA, Khrebtukova I, Loring JF, Laurent LC, Schroth GP & Sandberg R (2012). Full-length mRNA-Seq from single-cell levels of RNA and individual circulating tumor cells. *Nat Biotechnol* **30**, 777–782.

Ribeiro MJ, Sacramento JF, Gonzalez C, Guarino MP, Monteiro EC & Conde SV (2013). Carotid body denervation prevents the development of insulin resistance and hypertension induced by hypercaloric diets. *Diabetes* **62**, 2905–2916.

Robinson MD, McCarthy DJ & Smyth GK (2010). edgeR: a Bioconductor package for differential expression analysis of digital gene expression data. *Bioinformatics* **26**, 139–140.

Robinson MD & Smyth GK (2008). Small-sample estimation of negative binomial dispersion, with applications to SAGE data. *Biostatistics* **9**, 321–332.

Rocher A, Caceres AI, Almaraz L & Gonzalez C (2009). EPAC signalling pathways are involved in low PO_2 chemoreception in carotid body chemoreceptor cells. *J Physiol* **587**, 4015–4027.

Roy A, Derakhshan F & Wilson RJ (2013). Stress peptide PACAP engages multiple signaling pathways within the carotid body to initiate excitatory responses in respiratory and sympathetic chemosensory afferents. *Am J Physiol Regul Integr Comp Physiol* **304**, R1070–R1084.

Saito H, Chi Q, Zhuang H, Matsunami H & Mainland JD (2009). Odor coding by a mammalian receptor repertoire. *Sci Signal* **2**, ra9.

Sanchez D, Lopez-Lopez JR, Pérez-García MT, Sanz-Alfayate G, Obeso A, Ganfornina MD & Gonzalez C (2002). Molecular identification of Kvalpha subunits that contribute to the oxygen-sensitive K^+ current of chemoreceptor cells of the rabbit carotid body. *J Physiol* **542**, 369–382.

Sato M (1994). Effects of CO_2, acetate and lowering extracellular pH on cytosolic Ca^{2+} and pH in cultured glomus cells of the newborn rabbit carotid body. *Neurosci Lett* **173**, 159–162.

Schultz HD & Li YL (2007). Carotid body function in heart failure. *Respir Physiol Neurobiol* **157**, 171–185.

Semenza GL (2012). Hypoxia-inducible factors in physiology and medicine. *Cell* **148**, 399–408.

Shalek AK, Satija R, Adiconis X, Gertner RS, Gaublomme JT, Raychowdhury R, Schwartz S, Yosef N, Malboeuf C, Lu D, Trombetta JJ, Gennert D, Gnirke A, Goren A, Hacohen N, Levin JZ, Park H & Regev A (2013). Single-cell transcriptomics reveals bimodality in expression and splicing in immune cells. *Nature* **498**, 236–240.

Shen Y, Yue F, McCleary DF, Ye Z, Edsall L, Kuan S, Wagner U, Dixon J, Lee L, Lobanenkov VV & Ren B (2012). A map of the cis-regulatory sequences in the mouse genome. *Nature* **488**, 116–120.

Streller T, Huckstorf C, Pfeiffer C & Acker H (2002). Unusual cytochrome a592 with low PO_2 affinity correlates as putative oxygen sensor with rat carotid body chemoreceptor discharge. *FASEB J* **16**, 1277–1279.

Summers BA, Overholt JL & Prabhakar NR (2000). Augmentation of L-type calcium current by hypoxia in rabbit carotid body glomus cells: evidence for a PKC-sensitive pathway. *J Neurophysiol* **84**, 1636–1644.

Takahashi N, Kozai D & Mori Y (2012). TRP channels: sensors and transducers of gasotransmitter signals. *Front Physiol* **3**, 324.

Tang F, Lao K & Surani MA (2011). Development and applications of single-cell transcriptome analysis. *Nat Methods* **8**, S6–S11.

Tello D, Balsa E, Acosta-Iborra B, Fuertes-Yebra E, Elorza A, Ordonez A, Corral-Escariz M, Soro I, Lopez-Bernardo E, Perales-Clemente E, Martinez-Ruiz A, Enriquez JA, Aragones J, Cadenas S & Landazuri MO (2011). Induction of the mitochondrial NDUFA4L2 protein by HIF-1alpha decreases oxygen consumption by inhibiting complex I activity. *Cell Metab* **14**, 768–779.

Tian H, Hammer RE, Matsumoto AM, Russell DW & McKnight SL (1998). The hypoxia-responsive transcription factor EPAS1 is essential for catecholamine homeostasis and protection against heart failure during embryonic development. *Genes Dev* **12**, 3320–3324.

Tremaroli V & Backhed F (2012). Functional interactions between the gut microbiota and host metabolism. *Nature* **489**, 242–249.

Turner PJ & Buckler KJ (2013). Oxygen and mitochondrial inhibitors modulate both monomeric and heteromeric TASK-1 and TASK-3 channels in mouse carotid body type-1 cells. *J Physiol* **591**, 5977–5998.

Wang D & Bodovitz S (2010). Single cell analysis: the new frontier in 'omics'. *Trends Biotechnol* **28**, 281–290.

Wang K, Li M & Hakonarson H (2010). ANNOVAR: functional annotation of genetic variants from high-throughput sequencing data. *Nucleic Acids Res* **38**, e164.

Wang WJ, Cheng GF, Dinger BG & Fidone SJ (1989). Effects of hypoxia on cyclic nucleotide formation in rabbit carotid body in vitro. *Neurosci Lett* **105**, 164–168.

Weber M, Pehl U, Breer H & Strotmann J (2002). Olfactory receptor expressed in ganglia of the autonomic nervous system. *J Neurosci Res* **68**, 176–184.

Wu AR, Neff NF, Kalisky T, Dalerba P, Treutlein B, Rothenberg ME, Mburu FM, Mantalas GL, Sim S, Clarke MF & Quake SR (2014). Quantitative assessment of single-cell RNA-sequencing methods. *Nat Methods* **11**, 41–46.

Wyatt CN, Mustard KJ, Pearson SA, Dallas ML, Atkinson L, Kumar P, Peers C, Hardie DG & Evans AM (2007). AMP-activated protein kinase mediates carotid body excitation by hypoxia. *J Biol Chem* **282**, 8092–8098.

Wyatt CN & Peers C (1993). Nicotinic acetylcholine receptors in isolated type I cells of the neonatal rat carotid body. *Neuroscience* **54**, 275–281.

Wyatt CN & Peers C (1995). Ca(2+)-activated K^+ channels in isolated type I cells of the neonatal rat carotid body. *J Physiol* **483**, 559–565.

Xu J, Xu F, Tse FW & Tse A (2005). ATP inhibits the hypoxia response in type I cells of rat carotid bodies. *J Neurochem* **92**, 1419–1430.

Yamamoto Y & Taniguchi K (2006). Expression of tandem P domain K^+ channel, TREK-1, in the rat carotid body. *J Histochem Cytochem* **54**, 467–472.

Yuan G, Vasavda C, Peng YJ, Makarenko VV, Raghuraman G, Nanduri J, Gadalla MM, Semenza GL, Kumar GK, Snyder SH & Prabhakar NR (2015). Protein kinase G-regulated production of H2S governs oxygen sensing. *Sci Signal* **8**, ra37.

Zhuang H & Matsunami H (2008). Evaluating cell-surface expression and measuring activation of mammalian odorant receptors in heterologous cells. *Nat Protoc* **3**, 1402–1413.

Additional information

Competing interests

The authors declare that they have no competing interests.

Author contributions

TZ and HM conceived and designed the project. TZ, MC, SK and HM performed the experiments and analysed the data. TZ and HM wrote the paper with input from all the authors. All authors have approved the final version of the manuscript and agree to be accountable for all aspects of the work. All persons designated as authors qualify for authorship, and all those who qualify for authorship are listed.

Funding

This work was supported by the Duke University Chancellor's Discovery Award Program and the NIH R01 grant (DC012095).

Acknowledgements

The authors thank Mengje Jessica Ni and Saima Akbar for technical assistance; Douglas Marchuk for sharing equipment; and Yue Jiang for helpful discussion and critically reviewing the manuscript.